The Tangential Drag of an Axially Oscillating Cylinder

by

Susan Schultz Tapscott

B.S., Swarthmore College
1972

Submitted in Partial Fulfillment of the
Requirements for the Degree of

Ocean Engineer

at the

Woods Hole Oceanographic Institution

and the

Massachusetts Institute of Technology

and for the degree of

Master of Science in Ocean Engineering

at the

Massachusetts Institute of Technology

September, 1975

Signature of Author... .....
Joint Program in Ocean Engineering, Woods Hole Oceanographic Institution - Massachusetts Institute of Technology, and the Department of Ocean Engineering, Massachusetts Institute of Technology, September 1975.

Certified by..... .....
Thesis Supervisor

....
Thesis Supervisor

Accepted by..... .....
Chairman, Joint Committee on Ocean Engineering, Woods Hole Oceanographic Institution - Massachusetts Institute of Technology

The Tangential Drag of an Axially Oscillating Cylinder

by

Susan Schultz Tapscott

Submitted to the Department of Ocean Engineering in partial fulfillment of the requirements for the degrees of Ocean Engineer and Master of Science in Ocean Engineering.

Abstract

An experimental investigation of the tangential drag of an axially oscillating cylinder is presented. Deep-sea mooring cables are oscillated sinusoidally at ocean wave amplitudes and frequencies, and experimental values of the tangential (friction) drag coefficient are obtained. The experimental values of the drag coefficient are compared with values predicted by the exact solution to the Navier-Stokes equations for a smooth cylinder in laminar flow. The experimental data reports drag coefficient values that are consistently higher than those predicted by the laminar theory. An attempt is made to interpret the discrepancies in terms of the effects of roughness and/or turbulence.

Thesis Supervisor: Patrick Leehey
Title: Professor of Ocean Engineering at the Massachusetts Institute of Technology

Thesis Supervisor: James W. Mavor, Jr.
Title: Mechanical Engineer at the Woods Hole Oceanographic Institution

ACKNOWLEDGMENTS

Many thanks to Mr. James Mavor for his continuing optimism about my experiments in the topsy-turvy program of ocean engineering education at the Woods Hole Oceanographic Institution .

I am grateful to Professor Patrick Leehey for his constructive criticisms and suggestions throughout the preparation of this thesis.

Very special thanks go out to the many people at Woods Hole Oceanographic Institution who gave freely of their experience, time, energy, and equipment to make this thesis possible; Mr. Arnold Sharp, Mr. Ted Spencer, Mr. James Sullivan, Mr. William Shultz, and Mr. David Simoneau.

Finally, I am grateful to my husband for his infinite patience and kindness.

TABLE OF CONTENTS

TABLE OF CONTENTS (Cont.)

NOTATION

A or A_i	(i^{th}) oscillation amplitude
a	cylinder radius
C_1, C_2	constants
C_T	tangential (friction) drag coefficient
D	pulley diameter
d	cylinder diameter
F_h	force amplitude measured at high water level
F_l	force amplitude measured at low water level
F_m	force amplitude measured at middle water level
F_T	tangential drag force
$f(a\alpha)$	$N_1(a\alpha)/N_0(a\alpha)$
h	characteristic height of cylinder surface roughness
i	$\sqrt{-1}$, "imaginary number"
k^2	$i\alpha^2$, separation constant
l	test sample length
l_{h-l}	total test sample length between high and low water levels
l_{h-m}	total test sample length between high and middle water levels
l_{m-l}	total test sample length between middle and low water levels
$N_0^{-1}(x)$	inverse function of $N_0(x)$
n_a	average needle bearing frequency
n_i	instantaneous needle bearing frequency
n_t	turbulence frequency

q	$\frac{h}{a}$, roughness ratio
RE	"the real part of"
Re	Reynolds number
Re_A	$\frac{A^2\omega}{\nu} = A^2\alpha^2$, Reynolds number using A
Re_a	$\frac{a^2\omega}{\nu} = a^2\alpha^2$, Reynolds number using a
(r, θ, z)	circular cylindrical coordinates
S/N	peak F_T/peak F_1, signal to noise ratio
s	area of cylinder surface roughness per unit length
T	oscillation period
T_o	tension in test sample
t	time
V_o	$A\omega$, peak cylinder velocity
(V_r, V_θ, V_z)	velocities in circular cylindrical coordinates
α^2	$\frac{\omega}{\nu}$
δ	boundary layer thickness
μ	viscosity (of water)
ν	kinematic viscosity (of water)
ρ	density (of water)
τ_{rz}	sheer stress on cylinder (due to axial flow)
ω	oscillation radian frequency

I. INTRODUCTION

A. Problem Statement and Motivation for Study

An experimental study of the tangential drag of an axially oscillating cylinder is presented. The oscillating cylinders are deep-sea mooring cables forced in the axial direction at amplitudes and frequencies normally encountered in ocean moorings. No attempt is made to study the fine structure of boundary layers or to perform extensive mathematical analysis of the flow conditions. Comparisons are made, however, between the forces predicted by a simple solution to the Navier-Stokes equations for the laminar case and the measured, experimental forces.

The motivation for studying the tangential drag of an axially oscillating cylinder comes from two sources: first, from an interest in deep-sea, surface mooring dynamics and, secondly, from the lack of adequate analytic or experimental study of the specific problem. My interest in the problem comes primarily from the first motivator, the field of mooring dynamics. It has been found in recent years that (oceanographic) surface moorings have a reliability of 54% compared to a reliability of 90% for subsurface moorings (Walden and Panicker, 1973) and that current velocities recorded by current meters placed at the same depths on surface and subsurface moorings indicate current energies that are consistently greater for surface than subsurface moorings (Gould and Sambuco, 1975). Hong (1972), in a mooring dynamics study, finds that a reliable estimate of the tangential drag coefficient is essential for determining the dynamic forces in surface moorings, with the frequency response function of the mooring being heavily dependent on

the choice of value of the tangential drag coefficient. Goeller and Laura (1971) also find the choice of tangential drag coefficient to be important as it has a significant effect on reducing dynamic forces in the vicinity of resonance. From these pieces of evidence, it appears that surface mooring dynamics, due to the sea surface boundary condition of the structure, are important to structural design and reliability and to oceanographic data quality.

B. Previous work

From studies, such as the four cited above, related to energy transfer from the sea surface to the mooring line, it has become apparent that several parameters in the analysis are not well-known. Tangential "external" damping coefficients are not the only ambiguous quantities, but "internal" material damping parameters of synthetic line (Hong, 1972; Goeller and Laura, 1971) are also unknown but important to the problem. A study that compares actual mooring motions with computer-predicted motions (Panicker et al, 1974) seems to show that, indeed, tangential drag on the mooring system has the tendency to reduce peaks at the natural frequency of the system in the case of the acceleration response. But, at best, it is possible to assign a tangential drag coefficient that is the value determined for cables or cylinders in uniform, axial flow. A tangential drag coefficient that is (oscillation) frequency and amplitude dependent does not exist to date (Yamamoto et al, 1974; Hong, 1972) and computer programs for mooring dynamics (Goodman et al, 1972; Kaplan et al, 1972; Sargent et al, 1972) presently use a tangential drag coefficient that is frequency and amplitude independent.

In regards to theoretical background, a related problem that has been solved for many years is that of the flow near an oscillating flat plate; Stokes' second problem (Schlichting, 1968). An exact solution of the Navier-Stokes equations can be performed for this case. For the axially oscillating cylinder, the analytical expression for the flowfield near the cylinder has recently been presented following Stokes (Stokes, 1901; Casarella and Laura, 1969; Hong, 1972). The Navier-Stokes equations, expressed in circular cylindrical coordinates, are solved for the laminar flow case. Using the laminar flow results, Yamamoto (Yamamoto et al, 1974) estimates the skin friction coefficient for axially oscillating cables. Assuming that curvature effects of cables are small, Yamamoto proceeds to derive an expression for the skin friction coefficient for the cable in turbulent flow conditions, based on the boundary layer of a flat plate. This is, to date, the extent of the theoretical work done for the flow near an axially oscillating cylinder. The laminar flowfield has been amply treated but the same is not true of the turbulent flowfield, probably the more likely condition for deep-sea moorings due to cable roughness factors and the fact that (large) normal flows and cable strumming are also typical of the flow conditions.

C. Method of Study

As stated above, the author does not intend to perform a mathematical study of the problem, but, rather, an experimental study. It was felt that a good experimental study of the problem would yield information that was much needed by and directly useful to those in the mooring dynamics field.

Further, the cylinders that are studied here are real mooring cables ranging from jacketed wire ropes to various sizes and types of synthetic lines. An experimental study of an ideally smooth cylinder would be of more value to the theoreticians but of less value to those designing mooring systems. It was felt that the jacketed wire rope came as close to being an ideally smooth cylinder as would any real-life engineering material.

The amplitudes and frequencies of oscillation chosen here also attempt to approximate the field conditions for deep-sea moorings. Sinusoidal oscillations ranging from 2.8 seconds to 18.5 seconds in period and .1 meter to .5 meters in (single) amplitude were used. Even larger oscillation amplitudes would have been used had it been practical. A Scotch yoke driving mechanism produced the sinusoidal oscillations, and data was taken using a strain gage ring dynamometer to measure force, a potentiometer to measure displacement, and strip chart and FM tape recorders for recording the data. The strip chart records were then analyzed, producing one set of results. The FM tape was played into another chart recorder, and that strip chart record (of much better quality than the first) was then analyzed. If a spectral analysis of the data or a digitized data record is ever desired, the FM tapes can be used in conjunction with the computer to obtain this information.

Following a presentation and analysis of the data, comparisons are made between the experimental results and theoretical predictions using the Casarella and Laura (1969) predictions for the comparison.

II. MATHEMATICAL ANALYSIS

As stated above, it is not the author's intention to perform an extensive mathematical study of the tangential drag of an axially oscillating cylinder. But one mathematical description of the flowfield will be presented here for later comparison with the experimental data. The assumptions inherent in the description and suggestions for future work will then be discussed. Finally, a dimensional analysis of the problem will be performed for later use with the experimental data.

A. Linear analysis - Exact solution to the Navier-Stokes equations

Casarella and Laura (1969) have presented an analytical expression for the viscous drag on a smooth rod undergoing axial and torsional oscillations. The following method of analysis comes originally from Stokes' work (Stokes, 1901) and only more recently from their work as applied to an infinite cylinder of radius (a) that is undergoing pure axial oscillations. Expressing the Navier-Stokes and continuity equations in circular cylindrical coordinates (r, θ, z) leads to the four equations given in Appendix 1. The following equations result after assuming that the flowfield is independent 1) of z because the cylinder has infinite length and 2) of θ due to symmetry, that V_r and its derivatives with respect to r are zero because of the boundary conditions at the cylinder ($V_r = 0$ at $r = a$) and the continuity equation, and that V_θ and its derivatives with respect to r are zero, also by symmetry:

$$(1) \qquad r^2 \frac{\partial^2 V_z}{\partial r^2} + r \frac{\partial V_z}{\partial r} - \frac{1}{\nu} r^2 \frac{\partial V_z}{\partial t} = 0 \quad .$$

By separating variables and letting $V_z = R(r)\ T(t)$ we find that

$$(2) \quad T(t) = e^{i\omega t} \ ,$$

the separation constant k^2 has a value

$$(3) \quad k^2 = i\alpha^2$$

$$(4) \quad \alpha^2 = \frac{\omega}{\nu} \ ,$$

and

$$(5) \quad r^2 \frac{d^2R}{dr^2} + r \frac{dR}{dr} - k^2r^2R = 0 \ ,$$

since $\frac{\partial V_z}{\partial t} = i\omega V_z$. The general solution to equation (5) is in terms of Kelvin functions (Carslaw and Jaeger, 1959) so that

$$(6) \quad R(r) = C_1 I_0(kr) + C_2 K_0(kr)$$

where C_1 and C_2 are constants. The total solution becomes

$$(7) \quad V_z(r,t) = R(r)\ T(t) = e^{i\omega t}\ (C_1 I_0(kr) + C_2 K_0(kr))$$

The two boundary conditions are

$$(8) \quad V_z(a,t) = V_0 \cos \omega t$$

$$(9) \quad V_z(\infty,t) = 0$$

Applying the boundary conditions we find that

$$(10) \quad V_z(r,t) = RE\left[V_0 e^{i\omega t} \frac{K_0(kr)}{K_0(ka)}\right]$$

where RE signifies "the real part of". The tangential drag force per unit length becomes

$$(11) \quad \frac{F(a,t)}{l} = -2\pi a\ \tau_{rz}\Big|_{r=a} = -2\pi a\mu \frac{\partial V_z}{\partial r}\Big|_{r=a}$$

$$(12)\quad \frac{F(a,t)}{l} = RE\left[2\pi a\mu k\, V_o e^{i\omega t}\, \frac{K_1(ka)}{K_o(ka)}\right]$$

Now, using the relationships (Abramowitz and Stegun, 1968)

$$(13)\quad \frac{d}{dr}\left(K_o(kr)\right) = -k\, K_1(kr)$$

$$(14)\quad \frac{d}{dr}\left(K_1(kr)\right) = -k\, K_o(kr) - \frac{1}{r} K_1(kr)$$

and

$$(15)\quad K_o(kr) = N_o(\alpha r)e^{i\phi_o(\alpha r)}$$

$$(16)\quad K_1(kr) = iN_1(\alpha r)e^{i\phi_1(\alpha r)}$$

equation (9) becomes

$$(17)\quad \frac{F(a,t)}{l} = 2\pi a\mu\alpha\, V_o\, \frac{N_1(\alpha a)}{N_o(\alpha a)}\, \cos\left(\omega t + \phi_1\, \alpha r - \phi_o\, \alpha r - \frac{\pi}{4}\right)$$

If desired, the above equations can be simplified if $\alpha a \gg 1$. Using asymptotic expansions (Abramowitz and Stegun, 1968) for $N_p(\alpha a)$ and $\phi_p(\alpha a)$ and neglecting terms of order $1/z$ or smaller, equation (17) becomes

$$(18)\quad \frac{F(a,t)}{l} = 2\pi a\mu\alpha\, V_o \cos\left(\omega t - \frac{3\pi}{4}\right)$$

The results obtained above are in exact solution of the Navier-Stokes equations for laminar flow. No assumptions about the size of the oscillation amplitude or any other parameter have been made. But the question then arises as to whether the flow is always laminar. A stability analysis of the governing equations would help to indicate if and under what conditions

turbulent flow might occur. Unfortunately, stability theory for the case at hand has not yet been developed (Orszag, 1975). The inside-out case, the stability of Poiseuille flow, has been studied to some extent (Grosch and Salwen, 1972), and the stability of the incompressible boundary layer of a flat plate in a mean flow undergoing small perturbations has also been the subject of considerable research (Obremski et al, 1969). So as a stability analysis of the flow near an axially oscillating cylinder does not exist and is beyond the scope of this paper, discussion on the possibility of a turbulent flowfield near the cylinder must resort to qualitative reasoning and specific reference to the experiments performed for this work.

The most obvious experimental cause for turbulence is the roughness of the oscillating cylinder. Unlike the ideal cylinder in the equations, real cylinders and especially real mooring line materials have surface roughness of varying degrees. One might expect that, turbulent flow aside, the tangential drag of an oscillating mooring line would be greater than that of a perfectly smooth cylinder. But at what point the rough surface becomes a turbulence stimulator is a very good question. Using another line of reasoning, a deep-sea surface mooring would sometimes have a turbulent flowfield in the axial direction because many moorings not only undergo axial oscillations but also are moored in a flow normal to the mooring line (i.e., currents). If the Reynolds number describing the normal flow $Re = \frac{VD}{\nu}$ becomes sufficiently high that turbulent flow occurs in the normal direction (with cable strumming also occurring at times), it is highly improbable that the flowfield in the tangential direction would remain laminar (or uniform).

If the flowfield is turbulent, the equations describing the flow become very complex and cannot be solved easily. Yamamoto (Yamamoto et al, 1974) avoided the difficult equations, asserting that since curvature effects of mooring cables are small for laminar flow, flow over a flat plate will give good estimates of the tangential (friction) drag coefficient on a cylinder (mooring line) for turbulent flow as well. It is doubtful, though, that the assertion about small curvature effects is always true for real mooring materials. For the statement to be true, one must presumably find that the ratio of boundary layer thickness to line radius is much less than one, or

$$(19) \quad \frac{\delta}{a} << 1 \quad .$$

Using Yamamoto's definition of boundary layer thickness (also see Schlichting, 1968) i.e., the distance at which the fluid velocity becomes 1% of that of the cylinder, and the frequencies, line radii, and kinematic viscosities encountered in the experiments performed here, the following calculations result:

The boundary layer thickness δ is defined as

$$(20) \quad \delta = \left[\frac{1}{\alpha} N_0^{-1}(.01\, N_0(\alpha a))\right] - a$$

where

$$.0165 \text{ ft.} \leq a \leq .0415 \text{ ft.}$$

$$1.07 \times 10^{-5} \text{ ft.}^2/\text{s} \leq \nu \leq 1.31 \times 10^{-5} \text{ ft.}^2/\text{s}$$

$$.340 \text{ rad./s} \leq \omega \leq 2.244 \text{ rad./s}$$

So for

$$\alpha a_{min} = (.0165 \text{ ft.}) \left[\frac{.340 \text{ rad./s}}{1.31 \times 10^{-5} \text{ ft.}^2/\text{s}} \right]^{1/2}$$

$$= 2.65$$

$$= \alpha^1_{min}$$

$$\alpha a_{max} = (.0415 \text{ ft.}) \left[\frac{2.244 \text{ rad./s}}{1.07 \times 10^{-5} \text{ ft.}^2/\text{s}} \right]^{1/2}$$

$$= 19.00$$

$$= \alpha^1_{max}$$

From tables (Abramowitz and Stegun, 1968),

$$N_o(\alpha^1_{min}) = .1143$$

$$N_o(\alpha^1_{max}) = 4.187 \times 10^{-7}$$

$$.01\ N_o(\alpha^1_{min}) = 1.143 \times 10^{-3}$$

$$.01\ N_o(\alpha^1_{max}) = 4.187 \times 10^{-9}$$

$$N_o^{-1}(1.143 \times 10^{-3}) \simeq 8.5$$

$$N_o^{-1}(4.187 \times 10^{-9}) \simeq 32$$

$$\delta_{min} = \left(\frac{1}{\alpha^1_{min}} (8.5) - .0165\right) \text{ ft.} = 3.6 \times 10^{-2} \text{ ft.}$$

$$\delta_{max} = \left(\frac{1}{\alpha^1_{max}} (32) - .0415\right) \text{ ft.} = 2.838 \times 10^{-2} \text{ ft.}$$

$$\left(\frac{\delta}{a}\right)_{min} \simeq 2.2$$

$$\left(\frac{\delta}{a}\right)_{max} \simeq .7 \quad .$$

$\therefore \frac{\delta}{a} \ll 1$ is not satisfied.

So it seems safe to conclude that comparing the flowfield around the cylinder to that of a flat plate is risky at best. And until a stability analysis is performed for the equations governing the axially oscillating cylinder, it will remain uncertain as to whether a turbulent flowfield would in fact be formed.

In conclusion, the main shortcoming of the mathematical analysis that exists to date for the axially oscillating cylinder is the lack of mathematical understanding of turbulent flow. A stability analysis of the problem would at least let us know whether or not turbulence might occur. And, secondly, in a more experimental vein, a better understanding of the effects of cylinder roughness on the tangential drag coefficient would be very helpful.

B. Dimensional analysis

In order to better understand the problem of the axially oscillating cylinder, a dimensional analysis of the problem will be performed here. Such an analysis is useful in choosing suitable dimensionless parameters for comparing experimental data and analytically predicted quantities. These dimensionless quantities characterize the problem. In the following analysis, we will find that the problem is defined by six dimensional parameters less three fundamental units, leaving three dimensionless parameters to be defined.

The six dimensional quantities defining the problem are an amplitude A, the cylinder radius a, density ρ, viscosity μ, and force F. The three

fundamental units (of which the six dimensional quantities are made) are mass, length, and time, leaving three dimensionless parameters to describe the flowfield. One dimensionless parameter has already been defined by the analytical solution to the problem, i.e., $a\alpha = a\sqrt{\frac{\omega}{\nu}}$, and if we define a tangential drag coefficient C_T as the second parameter, we find the third parameter in the following manner: C_T is defined as

$$(21) \quad C_T = \frac{(F_T/l)}{\rho\pi 2a(A\omega^2)}$$

and

$$(22) \quad f(a\alpha) = \frac{N_1(a\alpha)}{N_0(a\alpha)}$$

so

$$C_T = \frac{\pi 2a\mu A\omega^2}{\pi\rho a(A\omega)^2} \quad f(a\alpha)$$

$$(23) \quad C_T = \frac{2a}{A} \quad \frac{1}{a\alpha} \quad f(a\alpha)$$

One may also develop C_T so that

$$(24) \quad C_T = \frac{2}{A\alpha} \quad f(a\alpha) \quad .$$

Now, from the two equations (23) and (24) above, the third parameter can be expressed in two different ways. The third parameter can be the ratio of the line diameter 2a to the oscillation amplitude A; 2a/A; or it can be the square root of a Reynolds number $A\alpha$ where $Re = A^2\omega/\nu = A^2\alpha^2$. The parameter derived from the mathematical analysis $a\alpha$ is also the square root of a

Reynolds number $Re = a^2\alpha^2$, and depending on which of the two so-called Reynolds numbers has more meaning in the context of data comparisons and analysis, either could be chosen as the abscissa for plots of C_T. If $a\alpha$ were chosen, then C_T $A/2a$ would be plotted versus $Re = a^2\alpha^2$. If $Re = A^2\alpha^2$ were chosen, then the ordinate would be C_T and $f(a\alpha)$ would be an implicit factor as C_T would not be a function only of $Re = A^2\alpha^2$. But in either case, the problem has been defined by three and only three dimensionless parameters.

In the context of experimental data, two additions to the dimensional analysis come to mind. The analysis outlined above pertains to an ideally smooth cylinder in laminar flow. Given experimental data and a suspicion that roughness or turbulence could be having an effect on the results, it would be desirable to isolate one effect from the other or to conclude that discrepancies between experimental data and theory were due solely to experimental error. It is impossible to perform a rigorous dimensional analysis incorporating roughness and turbulence effects because, unlike the previous dimensional analysis, there is no theoretical framework into which we can fit roughness and/or turbulence parameters. Hence, a qualitative dimensional analysis for roughness and turbulence will be presented and further disucssion will take place in Chapter IV in the context of data analysis.

Roughness may be characterized by either one or two quantities in addition to the original list of six dimensional quantities discussed above. At a minimum, some sort of height parameter h characterizing the surface roughness would be included, and a dimensionless parameter that might

result would be the ratio of roughness height h to cylinder radius a, the roughness ratio $q = h/a$. For a more complete description of the roughness, a second dimensional quantity dealing with the amount of surface area per unit length s occupied by the roughness could be added to the list of seven dimensional quantities. This would create a fifth dimensionless ratio, probably a ratio of roughness surface area to total surface area of the cylinder or $s/2\pi a$. The exact mathematical relationship among the five dimensional quantities C_T, $A\alpha$, $a\alpha$, h/a, and $s/2\pi a$ cannot be determined without additional mathematical theories or, perhaps, experimental data.

Turbulence is more difficult to describe in a dimensional analysis than is roughness. Again, without theory or experimental data, an exact mathematical analysis is impossible. But one might think about the quantity that best characterizes a turbulent flowfield. Usually a Reynolds number is used to indicate whether or not a flowfield should be turbulent. But such a Reynolds number is used with hindsight, usually from experimental observations. In the cases of (tangential) flow near a flat plate or in a pipe, the friction drag coefficient increases when transition and turbulence occur, producing curves of C_T versus Reynolds number that also have shallower slopes than in the laminar flow case (Schlichting, 1968; Hoerner, 1965). Roughness produces still shallower curves and larger drag coefficients. Further discussion of turbulence and roughness will occur in conjunction with the experimental data.

III. THE EXPERIMENT

A description of the experiment follows and consists of three parts: the overall configuration of the system, a description of the measuring and data-recording components of the system, and the design considerations involved in choosing the system described here.

A. Configuration

The experimental system is designed to make a force difference measurement by measuring the force while oscillating a cylinder with no water around it and then again when it is immersed in (fresh) water. Figure 1 shows the experimental set-up. The main system components are a cylindrical, vertical axis tank in which are mounted four large pulleys, two at the top and two at the bottom of the tank, a continuous test sample of mooring line that goes around the pulleys, a Scotch yoke that forces the line to move sinusoidally, a strain gaged ring dynamometer placed in-line in the forcing rod between the Scotch yoke and the test sample, and various data recording devices. The vertical tank is about 12 feet high and 5 feet in diameter with one base on the ground next to the Blake Building at the Woods Hole Oceanographic Institution (see Figures 2 and 3). The tank is approachable at its top by means of a ramp leading to the building. The Scotch yoke is mounted on the ramp next to the tank top and a forcing rod extends out over the tank to its attachment point on the rope. The attachment point occurs at the junction of the two ends of the rope, which are held together in tension by means of turnbuckles. In-line with the forcing rod is an aluminum loop upon which are mounted four

strain gages. The water level in the tank is first adjusted to barely cover the two pulleys mounted on the bottom of the tank. The first set of tests is then performed for the given rope sample, using the oscillation frequencies and amplitudes that have been chosen. The water level is then increased until it is just below the top two pulleys, and the oscillations are once again performed, giving the second set of tests for that sample. The strain gage dynamometer measures the force needed to oscillate the whole system of the pulleys and the rope, and the difference between the forces necessary to move the rope through the water and through the air is the tangential drag force on the rope.

Precise dimensions and specifications of the system are as follows: the tank height is 12.0 feet and its diameter is 5.3 feet. The pulleys are 11.6 inches in diameter and are made of PVC (polyvinylchloride) that is 1 inch thick. They run on 1/2 inch stainless steel shafts and sixteen 1/8 inch stainless steel needle bearings. Two collars hold the needles in their housings in each pulley (see Figure 4). The pulleys were designed to be as frictionless as possible.

Each test sample of line was cut to a precise length. The line was kept under about 50 pounds of tension to preclude transverse vibrations in the two, long, vertical sections of line. The tensioning was performed by the turnbuckles holding the rope ends together, and cutting exact, precalculated rope lengths was very important. As the synthetic lines tended to stretch, their cut lengths were shorter than those of the same diameter wire rope to allow room for stretching. The rope ends were terminated by potting them with epoxy in 1 inch lengths of thin-walled, 1 inch diameter

tubing. It was then possible to drill a hole through each termination and insert a threaded rod for attaching the turnbuckles (see Figure 5). The separations between pulleys and change in water level are given in Figure 1. From these distances, we see that the actual change in water level, or one-half the length of line over which we measure hydrodynamic drag, is 20.75 feet/2 or 10.38 feet.

The Scotch yoke drives the system through a forcing rod that is about 5.5 feet long. This "rod" is a very light weight (.43 pounds) aluminum tube that is 1 inch in diameter. One end is attached to the test sample and the other to the strain gage loop which is about 4.5 inches in diameter. On a diameter, across from the forcing pipe, the loop is attached to the Scotch yoke itself and the forcing rod is thereby continuous. The displacement of the center of the yoke is measured by a rotary potentiometer that is turned by gears running along a chain. The potentiometer (displacement) and strain gage loop (force) outputs are recorded on a two-channel strip chart recorder and on two of four channels on an FM tape recorder. The third tape channel is used for a time code from a time code generator, and the fourth channel is used for a voice record.

B. Measurements

Four strain gages mounted on a loop are used to measure the force required to oscillate the rope (see Figure 6). The loop is aluminum 7075 T6 with a yield strength of 70,000 pounds per square inch. The important force measurement in this experiment is the <u>difference</u> in force measurements between the high and low water level tests for each rope sample. In that this force

difference may be as small as 5-10% of the total measured force at either water level, it is necessary to approximately estimate the expected total force, excepting the drag, i.e., inertia forces and friction forces plus the other non-drag forces that occur. When these forces have been predicted, it then becomes possible to design the strain gage loop to be as sensitive as possible and strong enough to prevent failure or inelastic behavior over the given force range. The smaller the range (and the inertia and friction forces) the better, and, for this experiment, a range of 0-15 pounds (with 10 pounds a more realistic maximum and 15 pounds a safer maximum) was predicted and used. Appendix 2 gives the calculations made for this prediction and Appendix 3 gives the calculations made in choosing the loop dimensions of a 4.532 inch diameter, a .531 inch width, and a .0618 inch wall thickness. More discussion of the forces that are measured follows in the next section.

A loop with four strain gages measuring bending stress was chosen over a bar measuring axial stress because of the loop's greater sensitivity. The four gages on the loop become the four arms of a bridge circuit (see Figure 7) and since the output signal is a differential measurement, temperature compensation for the gages is inherent in the configuration. The gages are placed in a bridge circuit in either of two instruments designed for the purpose; for static testing of the strain gage loop, a Baldwin SR-4 strain gage indicator was used. It provided the 12 volts DC across the bridge and was capable of sensing ± 2 micro-inches per inch or, in this case, ± .003 pounds. For the actual tests and for static calibration runs, an MFE, model M-22CAHA, strip chart recorder was used. The chart recorder is a two-channel recorder and also places the gages in its own internal 12 volt

bridge circuit. The signal from the strain gage loop was recorded on one channel of this chart recorder and also on the first channel of the Sony FM tape recorder via a simple amplifier circuit (see Figure 8) for future processing.

Static calibration runs were done with the loop using known weights to apply a tensile or compressive load to the loop (see Figure 9). The chart and tape recorders each produced a calibration curve and these are given in Figures 10 and 11. As the highest test frequency was to be about .3 c/s it was felt that is was unnecessary to perform a dynamic calibration of the strain gage loop. The 3 dB down point for the chart recorder frequency response was 45 Hz, and the 2 dB down point for the tape recorder was 5 kHz.

The other measurement that was made was the displacement of the Scotch yoke driving point. This was done with a rotary potentiometer that was turned by gears running along a chain as the yoke moved. The 12 volt power supply of the other channel of the chart recorder and a simple voltage divider circuit (see Figure 12) enabled the displacement to be recorded simultaneously with the force on the second channels of both the chart and tape recorders. Again, dynamic calibration was not used for the potentiometer and chart and tape calibration curves were obtained by static calibration.

The other two tape channels were used for a time code and voice records, respectively, as mentioned before. The time code was included so that computer interfacing would be easier if and when spectral analysis of digitizing of the data were performed. The tape records of force and

displacement were also played back into a second chart recorder, a Hewlett-Packard 7100B strip chart recorder that was of better quality than the MFE chart recorder. The H-P recorder was not always available, so it was not possible to substitute it for the MFE recorder. Also, the MFE recorder was extremely useful for checking the force and displacement records as the experiment was going on as it was small, used little chart paper, and was easy to use. Its most important function, though, was in providing the proper bridge circuit for the specific type of strain gage used on the loop. But the H-P chart records were of much better quality for data analysis, so they form the basis for the "Data" chapter that follows.

C. Design considerations

The tangential drag of a cylinder in constant, axial flow is small compared to, say, the normal drag of a cylinder in constant normal flow, so it was assumed that in the oscillatory case, the drag force would also be of a small order of magnitude. With this very much in mind, it was necessary to design an experiment that allowed small forces to be detected. A few basic thoughts come to mind. The smaller the test sample, in length and in diameter, the smaller the drag force. The smaller the oscillation amplitude and frequency, again (presumably), the smaller the drag force and also the less realistic the experiment. If a long test sample is used, say, on the order of feet or tens of feet, then, if it were mounted horizontally, the line shape could change to that of a catenary and perhaps cause

the hydrodynamic problem to change, too. A short sample, though, mounted horizontally, would be less satisfactory than a long one in that a short sample would generate less total force, end effects would perhaps become important, and large oscillation amplitudes would be impossible if the amplitude to line length ratio is maintained to make the line effectively infinite in length. A vertical mounting that eliminated the catenary problem was considered superior. The length of the test sample is important once again because the vertical mounting of a long sample would require a very deep tank. A short, vertical test sample would have the same disadvantages as a short, horizontal test sample.

The purpose of the experiment is the detection of the tangential drag force. Even with extremely sophisticated instrumentation and test set-ups in a propeller tunnel, the problem is difficult. Using a single length of test sample, it is difficult to avoid having to make a differential measurement of some sort. One way to make a differential measurement would be to measure axial force at each end of the oscillating cylinder and attribute the difference in force to the drag on the cylinder between the points of measurement. This type of measurement requires very accurate zeroing of each force gage and a lack of zero drift during the experiment. In order to avoid this type of problem, one must make only one measurement of force. One way to do this would be to mount the test sample in such a way that it was not actually oscillated directly, but, rather, the mount to which it was attached was oscillated, and the relative force between the sample and the mount would become the drag force directly.

After considering the things listed above, the experiment was designed. The sample length was increased by using the four pulleys in such a way that the long, vertical lengths gave an effective sample length of about 20 feet in a 12-foot deep tank. The largest oscillation amplitude permitted by the tank and by the available sinusoidal drive was .5 meters (1 meter peak to peak), small enough to have the sample effectively infinite in length but large enough to be a real, ocean wave amplitude. Another advantage of the four-pulley, continuous set-up is its symmetry, i.e., as one vertical section is moving up through the water surface the other vertical section is moving down through the water surface, with the net surface-piercing force being constant from one-half wavelength to the next. Also, the pulley spacing and proximity to the walls of the tank was the maximum allowed by the tank for a maximum sample length. The distance from a pulley to the wall was chosen after boundary layer thickness calculations had been performed (as in the mathematical analysis chapter).

The most practical scheme for measuring the drag force seemed to be the one that was finally used and has been roughly described above. The idea of using two water levels and measuring force outside of the continuous, tensioned sample seemed to have many advantages. First, if an in-line measurement were attempted, it would have to be made using the tension in the line in some way. As it was calculated that a tension of at least 20 pounds was needed in order to prevent transverse vibrations in the long, vertical line sections, (see Appendix 4) any drag force would have to be measured on top of that tension, making it a very small percentage of the total measured force. It was decided to make the measurement in the forcing

rod outside the line so as to measure as small an extraneous force as possible. The extraneous force then became a combination of the inertia force of the system, the friction, the hydrodynamic drag of the two bottom-mounted pulleys, and the surface-piercing effects of the two vertical lines, all of which seemed to total to much less than the tension in the line (see Appendix 2). Also, it became unnecessary to actually place any measuring device or electronic gear directly on the test sample or in the water.

In regards to the tension of the line around the pulleys, the minimum tension was chosen as explained above. But in addition to the possible vibration problem, it was desired that any change in tension due to a weight change in the line as it was submerged be kept as small as possible compared to the line tension. As various types of line (wire and synthetics) were being tested and some of the larger diameter synthetics could undergo considerable weight per unit length changes from dry weight to neutrally buoyant in the water (see Table 1), it was desired that the tension be high enough to make these changes appear small by comparison. As the friction in the pulleys increases with line tension and the friction effect was to be removed by making the force measurement at two water levels, a large friction change relative to line tension, due to a weight change, was undesirable. Hence, a tension of 50 pounds was chosen as being large enough in this experiment.

Finally, the ring dynamometer was chosen as the force measuring device because it was very satisfactory for the job, simple and cheap. Commercial

force gages with the necessary sensitivity and range cost in excess of $400, often needed accompanying read-out equipment (amplifiers, etc.), and seemed to be no more satisfactory than the ring dynamometer. The potentiometer that measured the Scotch yoke displacement had been installed previously on the yoke and was used as it was. And the Scotch yoke itself was used as the driving mechanism because it was felt that a sinusoid was a good approximation to ocean waves and also best for comparison with theoretical predictions, most of which use sinusoidal oscillations.

IV. DATA

The experimental data will be introduced in the following manner: first, each data set will be presented in conjunction with the specifications of the particular experiment. The over-all characteristics of the data will be analyzed, and finally, a detailed look at the tangential drag coefficient data as compared to the theoretical predictions will occur.

A. Presentation of data

A total of seven experiments were performed, testing four different samples of mooring cables, and four different fresh water temperatures (viscosities and densities) had been encountered by the end of the testing period. The general experimental procedure outlined here applies to each data set below, unless otherwise noted.

Experimental procedure:

1. The test sample was mounted and tensioned around the four pulleys, and the Scotch Yoke and recording equipment were placed in position.
2. The water level in the tank was adjusted to the low water level; i.e., just covering the bottom two pulleys, for the first test series, and to the highest water level for the other test series for that sample. The same oscillation amplitudes and frequencies were used at each water level.
3. In a particular test series (low or high water level), oscillations progressed from large amplitudes to small amplitudes, low frequencies to high frequencies.

At a given amplitude, the lowest possible frequency was used for, say, N1 cycles and the frequency was then increased to the second frequency where it continued for N2 cycles, and so on to the highest test frequency. The Scotch Yoke was not stopped between the different frequencies and each successive frequency was higher than the previous frequency. The Scotch Yoke was stopped only to allow the amplitude setting to be changed (decreased).

4. Occasionally, a third series of tests was performed in addition to the low and high water level tests. A second series of low water level tests could be performed, after lowering the water level from high to low water, in order to check the original low water tests for reproducibility. Also, a mid-water depth test series could be performed with the water level somewhere between the high and low water levels, also to lend credibility to the data.
5. The water temperature was checked during the test period in order to determine the water viscosity and density.
6. The two series of tests, one each from the low and high water levels, were compared to yield the tangential drag force for the rope sample being tested.

Data processing:

1. Each series of tests for a given rope sample generated a force record for the oscillation amplitudes and frequencies that had been applied at that water level. The tape record of the force was played into a Hewlett-Packard chart recorder and the resulting chart record was analyzed.
2. First, the curves were smoothed, if necessary, and secondly, the peak to peak amplitudes of the resulting waveforms were measured and recorded. For a given oscillation amplitude and frequency, these amplitude values were averaged over the number of data cycles obtained, and the single resulting value was compared with the corresponding value from the other water level(s).
3. The difference between the high and low average force amplitudes, $(F_h - F_l)$, when reduced to the proper single amplitude force, yielded the peak tangential drag force for that test sample at each oscillation amplitude and frequency.
4. The resulting data points were compared with the values predicted by the exact solution to the Navier-Stokes equations.

Keeping in mind the brief outlines given above, a short definition of terms follows here. In the presentation of data, "high" or "h" denotes the water level of the completely filled tank, and "low" or "l" denotes the water level that just covers the bottom two pulleys in the tank. Any intermediate water level will be defined as it occurs and is denoted by "m". The rope length is considered to be the sum of the two vertical lengths of immersed sample, using the low water level as a zero reference. l_{h-l} denotes the rope length between the high and low water levels, l_{h-m} the rope length between the high and mid-water levels, and l_{m-l} the rope length between the mid and low water levels. The oscillation amplitude and all forces are single, maximum amplitudes and are not peak to peak measurements. All test samples are numbered and refer to entries in Table 1. Table 2 lists the density and viscosities (viscosity and kinematic viscosity) of the fresh water in the tank for the water temperatures that were encountered. The mathematical equations used for predicting C_T and F_T from the Navier-Stokes equations are given below, as are the equations used in calculating C_T from the force data (F_T) obtained in the experiments. From Section II-A, the maximum value of F(a,t) is

$$(25) \quad F_T = 2\pi\mu l(A\omega)a\alpha \quad f(a\alpha)$$

where $\alpha = \sqrt{\frac{\omega}{\nu}}$ and $f(a\alpha) = \frac{N_1(a\alpha)}{N_0(a\alpha)}$

$$(26) \quad C_T = \frac{F_T}{\frac{1}{2}\rho 2\pi a l (A\omega)^2}$$

$$(27) \quad C_T = \left(\frac{2}{A\alpha}\right) f(a\alpha) \quad .$$

Using the data for the tangential drag force it is possible to calculate C_T from equation (26) above, substituting the experimentally determined force value for F_T and using the proper values for the water density, rope radius, rope length, and oscillation amplitude and radian frequency. The experimental data is presented in Tables 3-1 through 3-7 and also includes the predicted, theoretical values for tangential drag forces and drag coefficients.

Figure 13 is a plot of $C_T \frac{A}{d}$ versus $Re_a = a^2 \frac{\omega}{\nu}$, comparing the data and theoretical values given above. Typical waveforms of the force data are shown in Figure 14 for various oscillation frequencies. Also, examples of the smoothed curves are given by the dotted lines in the same figure. Typical waveforms from the displacement records are shown in Figure 15. A discussion of the force waveforms follows in the next section of the chapter.

B. Analysis

First of all, a quick scan of Figure 13 reveals that the data does not quite predict the theory in these experiments. The comparison between theory and data will be discussed in the next section of this chapter, and the present analysis section will be devoted to a discussion of the data as it stands by itself. A few other general statements that can be made regarding the data are that the data seems internally consistent; i.e., the same rope sample produces the same experimental force data from test to test, more data has been obtained from larger diameter test samples than smaller, and there is more data at higher than lower frequencies. With these observations in mind, a more detailed analysis of the data follows here.

It seems logical to begin with a look at the raw data. Figure 14 shows that the force waveform changes with oscillation frequency, progressing from almost a square wave to an approximate sinusoid as the frequency increases. For all waveforms there is some higher frequency noise superposed on the basic (smoothed) wave. First of all, as the displacement applied by the Scotch Yoke is a pure sinusoid (see Figure 15), one would expect the measured driving force to be sinusoidal also. As it is <u>not</u> sinusoidal, one must consider why it is not. First, if the mechanical tolerances of the Scotch Yoke are sloppy, it is not difficult to generate higher harmonics and a force waveform that is not a pure sinusoid (Crandall et al, 1963) even though the displacement waveform appears to be perfectly sinusoidal. By the time a second derivative record is generated, slight imperfections in the displacement waveform will have become very noticeable. But the force waveforms seen in Figure 14 are not only the result of slight imperfectons in the displacement waveform. After much thought about the experimental set-up, friction in the four pulleys seems to be of major concern.

Although the pulleys were intended to be frictionless, they were not. They were extremely frictionless with no load on them; i.e., with zero tension in the rope test sample. But as the tension was increased, the friction increased also. It was possible to measure a starting friction for the four pulleys by attaching a very sensitive spring dynamometer to the rope at the point where the turnbuckles joined the two rope ends together, in place of the forcing rod. The starting friction varied as a function of rope tension, increasing when the tension was increased, and the same effect could be observed by loading a single pulley in the laboratory. In that a very flexible string could be tensioned around the pulleys and cause greater

friction with increased tension, it seemed to be bearing friction in the pulleys rather than an increase in the energy required to bend the test sample around the pulleys that created a greater resisting force to be overcome.

It is interesting to speculate on a model for the type of friction that would generate the waveforms in Figure 14 given sinusoidal displacement and velocity functions. Figure 16 shows some typical models of friction force versus velocity and the resulting friction force and friction plus inertia force for a sinusoidal velocity. After playing with various friction models, Figure 17 gives a model which seems to be able to generate curves very similar to those in Figure 14. It would be possible, of course, to construct very complicated friction models to exactly generate the observed data, but that is not the purpose of this exercise. Rather, Figure 17 seems to contribute to a basic understanding of the problem. Only the smoothed waveforms in Figure 14 have been predicted here, and possible reasons for the higher frequency noise will be presented in the following paragraphs.

The simple friction model in Figure 17 seems to confirm that the observed friction is of considerable magnitude and is not at all of the type shown in Figure 16-1 which predicts a high starting friction followed by a much lower kinetic friction as soon as the body is in motion. Also, the model in Figure 16-2 would almost match the data waveform progression as the inertia term was increased except that there can never be the reversals observed on the sides of the higher frequency waveforms. Unfortunately, not much is known about friction as it is related to oscillatory motions, but from the fairly good match between a simple friction model and the

data waveform, it would seem possible to attribute the non-sinusoidal form of the force data to friction. And if the explanation is correct it is also easier to understand why it was difficult to distinguish a very small tangential drag force on top of a very large friction force at low forcing frequencies.

The higher frequency noise superposed on the smoothed force waveform is also of concern. The mechanical system was by no means vibration free, and it is also remotely possible that the higher frequencies in the system could come from the hydrodynamics of the oscillating cylinder. The most likely source of mechanical vibration (with no obvious vibrations observed) is bearing noise from the needle bearings in the pulleys. It is possible to calculate the "needle frequency" or number of needles passing a reference point per second per pulley. There are sixteen needles in each pulley, and using simple geometry it is possible to calculate an instantaneous needle frequency of the form

$$(28) \quad n_i = \frac{16}{\pi D} \frac{dx}{dt} \qquad (c/s)$$

where x is the sinusoidal displacement, so that

$$(29) \quad n_i = \frac{16A\omega}{\pi D} \cos(\omega t) \ (c/s)$$

if $x = A\sin(\omega t)$.

But as an instantaneous observation of frequency is difficult to make, an average needle frequency is of more value. Then, integrating n_i over one-half cycle and dividing by $\frac{T}{2}$ we find that the average needle frequency n_a is

$$(30) \quad n_a = \frac{64A}{\pi DT} \qquad (c/s)$$

Using force waveforms from several sets of data and observing the higher frequency noise on the slowly changing portions of the force curves (peaks), Table 4 compares observed frequency with a computed needle frequency. The lower frequency data is analyzed using n_a for comparison, as the waveform is close to square. The two higher frequencies, T=3.6 s. and 2.8 s., are better understood when n_i, averaged over a suitable time interval, is used for comparison. In order to choose a suitable time interval over which to integrate, it is important to know the exact phase relationship between the displacement and the force. Based on the close agreement between the predicted bearing frequencies and the observed high frequencies, it seems fair to attribute the high frequency noise to bearing noise. This is an important conclusion as it would seem to justify the smoothing of the force data during the data processing.

One final comment may be made regarding a hydrodynamic high frequency in the experiment. Turbulent flow can be modeled as a mean flow plus a small perturbation that has some frequency n_t. The perturbation frequency n_t could be high relative to the forcing frequency and might be observed in the force measurement as high frequency noise. But without adequate experimental observations of turbulence or a theoretical (stability) analysis, it would be difficult to attribute high frequency noise to this cause. Also, with good agreement between predicted bearing frequencies and the observed high frequencies, further speculation on the source of the high frequency noise is not really necessary.

Explanations have now been made for the various data waveforms, leaving the actual data values as the next topic of discussion. Earlier it was observed that the data seems to be internally consistent, with one rope

sample producing the same experimental data in tests at different water temperatures and times. Sample 4 was tested in three different water temperatures at kinematic viscosities that varied from 1.31 to .95 ft.^{2}/s, a factor of .72. The rope was remounted on the pulleys for each test, so that the pre-tensioning was slightly different each time, and the tests took place over a period of time of two months. But from test to test the data is compatible (see the test results), with each new data set reinforcing the previous one(s). Also, for several of the four rope samples tested, at least two different oscillation amplitudes were used, producing many different combinations of amplitude and frequency; i.e., velocity. The data is compatible among the different velocities and is consistent for a large amplitude, low frequency combination or a smaller amplitude, higher frequency combination, both of which create the same velocity.

Further proof of the internal consistency and reliability of the data is shown by the results of Test 6 (Table 3-6) where low, middle, and high water tests were performed. The middle water level was almost exactly halfway between the low and high water levels with l_{h-m} = 10.66 and l_{m-l} = 10.10 feet (l_{h-l} = 20.75 feet), where "m" denotes "middle water level". Three sets of drag forces were obtained (see the third item in the data processing procedure in Section A of this chapter): one for the low to middle water line length (F_m-F_l), one for the middle to high water line length (F_h-F_m), and one for the low to high water line length (F_h-F_l). Figure 18 plots experimental drag force versus length of line immersed for four oscillation periods, using the low water level as a zero length immersed reference. The fact that (F_m-F_l) and (F_h-F_m) come close to having

values that are, respectively, $\frac{10.10}{20.75}$ (F_h-F_l) and $\frac{10.66}{20.75}$ (F_h-F_l) shows that the relationship between experimental drag force and line length immersed is linear as it should be, lending further credence to the experimental data.

The test results in the previous section include a signal to noise ratio S/N for each data point. The ratio is defined as the ratio of peak tangential drag force to the peak low water force measurement at that amplitude and frequency. It is not surprising that the S/N ratio is on the small side, varying from .006 to .109 and averaging .048 or about one out of twenty. The tangential drag force is not large, and even though the S/N ratios are low, the data still appears to be reliable and meaningful.

Leading into an analysis of experimental error and offering one more reason to justify the smoothing of the force waveform, a quick look at the hand-done nature of the data processing will be taken here. It could be argued that hand-done data processing could lead to a bias in the experimental results. As a check on this possibility and on data reliability, several of the magnetic data tapes were analyzed on a waveform eductor. The eductor is an electronic package that produces an average waveform, constructed from a large number of data cylces at one frequency and amplitude. Samples of these results showing the high and low water average waveforms superposed on each other (Figure 19) indicate that, indeed, there is an observable hydrodynamic drag force even with a machine doing the data processing. The area between the two waveforms is the product of the drag force and the time and using a plenimeter, this area has been computed and an average height or drag force calculated. The drag force obtained using the

plenimeter and the drag force from the hand-processed data are compared in Figure 19. The close agreement between the forces calculated in two different ways helps to confirm that the data processed by hand is not biased, that there does really seem to be a drag force present on top of the noise, and that smoothed data predicts the same drag force as the unsmoothed waveform eductor data. Another interesting observation that can be made is that the high frequency noise never seemed to average out, even with a large number of data cycles. As the noise seemed to be present for both the low and high water data, and in phase, this allowed the smoothed and unsmoothed force data to predict the same drag forces.

The subject of experimental error is a complicated one. The following discussion will enumerate causes for error and try to estimate the amount of error contributed in each case. First, in the data acquisition procedure, error may enter due to changes in the experimental set-up during testing. If the tension in the rope sample changes significantly, it may cause the friction in the pulleys to vary from low to high water, thereby changing a quantity that is supposedly constant throughout the test. A tension change could occur if a test sample were to stretch or change its weight in some way. A weight change due to buoyancy effects does occur between low and high water, but it should not contribute to a change in the friction for the following reasons: As the rope sample is continuous around the four identical pulleys and the weight change between high and low water is equal in the two vertical test sections of rope, the tension around the top two pulleys is decreased by an amount equal to the weight change in one vertical section and increased by the same amount in the bottom two pulleys. Assuming that a small increase or decrease in tension produces a linear

increase or decrease in pulley friction, the effects of a weight change on pulley friction are cancelled around the four pulleys.

On the other hand, if the nylon were to stretch during the time between a low and high water test (four hours with the low water test performed first), a decrease in pulley friction would be felt in all four pulleys. It is not possible to calculate the rope stretch and resulting friction change that might occur during an experiment. Creep and creep rates are not well-documented for synthetic lines, especially at such low tensions (fifty pounds or less). According to Berteaux (Berteaux and Chhabra, 1973) for used nylon, the strain at the tensions used in the experiment would be less than 2% or about 1.6% for Sample 3 and .5% for Sample 4. This would mean a length change of about .5 and .2 feet, respectively, for the two types of line. From observations during the experiments, stretching did occur for both nylon samples but was easily observed only after times on the order of days. On the other hand, it is the author's qualitative belief that stretching and/or weight changes did have an effect on the nylon data quality, especially at low frequencies where a friction change would have been most noticeable.

But based on a lack of understanding of the behavior of synthetics and the exact tension-friction relationship in the pulleys, a qualitative judgment of experimental error will be made for the problem of changing friction. For the nylon test samples, if stretching did occur during the test period it would have decreased the friction in the four pulleys, tending to cause an underestimation of the tangential drag force if not taken into account. Based on the reasoning above, a somewhat arbitrary

choice of .03 pounds of underestimated force will be considered the error of underestimation for both Samples 3 and 4. As the wire rope does not stretch, no underestimation error will be assigned.

Another source of experimental error is that due to the measurement of the peak to peak force on the chart record. The actual measurement is limited by the ability to read to $\pm$ .01 cm. or $\pm$ .012 pounds. But the total error after reading over a number of data cycles may be much greater. One way to estimate this error is to return to the comparisons between the force data obtained from the waveform eductor and the hand-processed data (Figure 19). Based on the difference between the two sets of results, the total data processing error seems to be more on the order of $\pm$ .03 pounds.

Finally, the other type of error that would enter the force data would be errors in calibration of the ring dynamometer. Based on the repeatability of calibration runs, an estimate of a total error of .02 pounds or $\pm$ .01 pounds seems reasonable, with the .02 pound error due to inexact calibration weights.

Totaling the errors itemized above, the force error for wire rope Samples 2 and 5 is $\pm$ .04 pounds and for nylon Samples 3 and 4 is + .07 pounds and -.04 pounds. Figure 20 shows the estimated errors in the drag coefficient data. Additional mention of the signal to noise ratio S/N might be appropriate at this time. The errors given above for each data point could be interpreted in the context of the S/N value for the point. It would be possible to think of the S/N ratio as a weighting factor to be applied to the error bars, with a diminution of the error bars allowed for high S/N ratios where the data point seems more "reliable".

C. Discussion

The previous section consisted of an analysis of the experimental data in regards to its waveforms, noise, S/N ratios, internal consistency, error functions, and other characteristics. A discussion of how best to compare experimental and theoretical values will first be presented. The tangential drag coefficient data will then be examined in comparison with the theoretical predictions made in Chapter II, and the discrepancies between the data and the theory will be discussed.

In order to have the best possible understanding of the data, appropriate dimensionless parameters should be used for comparing the theoretical predictions and the data. Returning once again to the discussion in Section B of Chapter II, it was pointed out that two of the three dimensionless parameters characterizing the problem are the parameters C_T and $a\alpha$. The third parameter could be chosen as either $\frac{A}{d}$ or $A\alpha$. Looking more closely at $a\alpha$, it has the physical meaning of the ratio of the cylinder radius to a boundary layer thickness. The quantity α is defined as $\alpha = \sqrt{\frac{\omega}{\nu}}$, and for Stokes' second problem of the oscillating flat plate, the boundary layer thickness δ is on the order of $\delta \simeq \frac{1}{\alpha} = \sqrt{\frac{\nu}{\omega}}$ (Schlichting, 1968). Hence, $a\alpha$ is a ratio of cylinder radius to boundary layer thickness. Although the boundary layer thickness for the oscillating cylinder cannot quite be approximated by the boundary layer thickness for the flat plate for the particular values of quantities encountered in these experiments (as shown in Chapter II), in the limit of a cylinder with a very large radius, $\sqrt{\frac{\nu}{\omega}}$ would become on the order of the boundary layer thickness. So in the flat plate limit, $a\alpha = \frac{a}{\delta}$ becomes the ratio of cylinder radius to boundary

layer thickness.

The dimensionless parameter $\frac{A}{d}$ is easily understood as being the ratio of oscillation amplitude to cylinder diameter. The quantity $A\alpha$ is not quite so easily interpreted, but if it is squared, becoming $A^2\alpha^2 = A^2 \frac{\omega}{\nu}$, it begins to look rather familar; it could be called a Reynolds number Re_A = (velocity)(length)/(kinematic viscosity) = $(A\omega)\frac{(A)}{\nu}$. Physically, it is easy to envision the cylinder velocity $A\omega$, a characteristic length A, and a ratio of inertial forces to viscous forces. This type of a Reynolds number would be used to describe the flowfield near a flat plate, for example. Now, returning to the quantity $a\alpha$, if it were squared it too could be a sort of Reynolds number as it is made of the same dimensional quantities as Re_A. But $Re_a = a^2\alpha^2$ does not have the same physical meaning as does Re_A. It is difficult to understand which velocity is represented by $a\omega$, and of which inertial and viscous forces we are speaking.

Having reviewed the physical interpretations of the dimensionless parameters, it now remains to choose the appropriate parameters for the comparisons between the experimental data and the laminar theory. Repeating equation (23) from Chapter II,

$$(23) \quad C_T = \left(\frac{2a}{A}\right)\left(\frac{1}{a\alpha}\right) f(a\alpha)$$

it can be rearranged as

$$(28) \quad C_T \frac{A}{2a} = f^1(a^2\alpha^2)$$

where $$f^1(a^2\alpha^2) = \frac{1}{\sqrt{a^2\alpha^2}} f(\sqrt{a^2\alpha^2}) .$$

$C_T \frac{A}{2a}$ is then only a function of $Re_a = a^2\alpha^2$, so data and theory could be compared in a plot of $C_T \frac{A}{d}$ versus Re_a. Equation (24) from Chapter II is repeated:

$$(24) \quad C_T = \frac{2}{A\alpha} f(a\alpha) \quad .$$

and C_T is a function of Re_A and Re_a. As above, (24) can be rearranged so that

$$(29) \quad C_T \frac{1}{f(a\alpha)} = f_A(A^2\alpha^2)$$

where $$f_A(A^2\alpha^2) = \frac{2}{\sqrt{A^2\alpha^2}}$$

and $C_T \frac{1}{f(a\alpha)}$ versus Re_A could be plotted for the experimental and theoretical values.

But which comparison has more meaning: $C_T \frac{A}{d}$ versus Re_a or $C_T \frac{1}{f(a\alpha)}$ versus Re_A? For those interested in fine-scale phenomena in the boundary layer, probably the comparison using Re_a has more significance. It implies that one might want to find the value of $C_T \frac{A}{d}$ given a certain ratio of cylinder radius to boundary layer thickness. On the other hand, a person interested in tangential drag coefficients in flows characterized by their (conventional) Ryenolds numbers might be attracted to the relationship between $C_T \frac{1}{f(a\alpha)}$ and Re_A or even to the relationship between C_T and Re_A. (As any plot of C_T versus Re_A is not independent of $f(a\alpha)$, a separate curve would be generated for each value of $f(a\alpha)$). In that a true Reynolds number characterizes several flowfields that will be contrasted with the flowfield near an axially oscillating cylinder in the next few pages, all new plots that are presented in this section will be of the form $C_T \frac{1}{f(a\alpha)}$ versus Re_A. It is interesting

to note, though, that C_T is almost independent of Re_a compared to Re_A. Because the quantity $f(a\alpha)$ is so close to 1.0 for all values of $a\alpha$ encountered in the experiments (see Table 3), instead of having a family of curves for different values of $f(a\alpha)$ when plotting C_T versus Re_A, the curves are so close together that they almost appear to be a single curve for Samples 3 and 4. Figure 21 shows the two lines that are the farthest apart for the Sample 3 and 4 nylon data and the line that is the most different from the nylon line, the Sample 2 wire rope line (smallest diameter).

Figures 13 and 22 show all the experimental data compared to the theoretical predictions in plots of $C_T \frac{A}{d}$ versus Re_a and $C_T \frac{1}{f(a\alpha)}$ versus Re_A, respectively. The plots are informative in showing that the experimental data does not agree with the theoretical predictions. What might affect the experimental results that is not accounted for in the theory? The first thing to look at is experimental error - might the data really agree with the theory, within experimental error? Glancing at Figure 20 which places error bars on the data points, the theoretical line does not fall within the error bars. Only if the error bars could be extended toward lower values of $C_T \left(\frac{A}{d} \right)$ or greatly increased in overall length would the data begin to include the theoretical line. The error estimates made in the previous section may be slightly off, but they would have to be changed drastically to encompass the theoretical line. And the argument made for underestimation of the nylon drag coefficient would not encourage the error bars to be extended downward only - by a factor of more than three for Sample 4. So it would seem that the discrepancies between data and theory are not mainly due to experimental error.

What other effects might cause the data to have values that are consistently so much larger than the predicted values? The suspicion is that

perhaps roughness and turbulence are causing the experimental data to disagree with the laminar flow theory for a smooth cylinder. But as we have no mathematical theory capable of incorporating roughness and turbulence effects into the problem, we shall try to incorporate their effects in a qualitative way.

Surface roughness is a very obscure engineering parameter, and it is not well defined for things other than flat plates, such as cables in axial flows. A single, dimensionless surface roughness parameter will be used here and is defined as the roughness ratio $q = \frac{h}{a}$ where h is the height of the characteristic surface protrusion (a is the radius of the line). In judging surface roughness, the two wire ropes look the same. Each has a polyethylene jacket over the wire and the bulges in the jacket due to the individual strands of wire seem to have about the same roughness ratio, q = .020, for the two samples. Since there are not many data points for either sample and they seem to indicate the same trend, the two sets of data are grouped together for this analysis. Samples 3 and 4 are both nylon ropes but are of different rope lays and diameters. Sample 3 is a plaited nylon rope and Sample 4 is a 3-strand, "twisted" nylon rope. The estimated roughness ratio for Sample 3 is q = .100 and for Sample 4 is q = .098, but since the two ropes have surfaces that look and feel very different, the fact that the roughness ratios are about equal is not necessarily significant. In a very qualitative way, Sample 3 has lots of irregular bumps compared to fewer, more ordered protrusions for Sample 4.

Looking at the friction drag coefficient C_T versus Reynolds number $Re = \frac{VL}{\nu}$ for a flat plate in steady flow or flow in a pipe (Schlichting, 1968), at a Reynolds number of about 10^5 transition occurs and the flow becomes turbulent. The slope of the line changes, becoming more shallow,

and the drag coefficient changes, becoming larger than it would have been had the flow remained laminar. Further, if roughness is added to the picture the slope of the line decreases still further, so that it lies anywhere between the turbulent theory line and the horizontal, and the drag coefficient is again increased (Schlichting, 1968; Hoerner, 1965). So in the hierarchy of lines, the "rough" lines lie above the turbulent theory line with slopes that are less than or equal to that of the turbulent theory line, and the turbulent theory line lies above the laminar theory line and has a shallower slope. There are also transition regions from laminar to turbulent flow and from turbulent to rough conditions.

First, in order to have a better look at the data, Figures 23 and 24 separate the data in Figure 22 into two groups, the data from Sample 4 and the data from Samples 2, 3, and 5, respectively. The logic behind the grouping of the data in these figures is to put rope samples with the same surface roughness together. Perhaps the data from Sample 3 should be included with that from Sample 4 since both are nylon ropes, but since there are so few data points from Sample 3, they are placed with the wire rope points from Samples 2 and 5 for higher visibility.

Figures 23 and 24 show least squares fit lines for the data. In Figure 23, the circled Sample 4 data was included in calculating the line and the uncircled data was not. In Figure 24, two lines are shown, one is for all the Sample 2 and 5 data and the other for the circled Sample 3 data. Comparing the data lines, Figure 25 superposes the three lines on a single grid, along with the theoretical line. The line with the shallowest slope is line 2, followed by line 3, the theoretical line, and line 1 in the progression from the shallowest to the steepest slope.

It is not necessarily valid to compare the flow near a tangentially oscillating cylinder to that near a flat plate as was seen in Chapter II. But perhaps the basic trends discussed in the paragraphs above could be helpful here. Samples 2 and 5 are polyethylene jacketed wire ropes and are the closest thing in the experiment to an ideally smooth cylinder. One might, therefore, expect the data from Samples 2 and 5 to lie the closest to the line predicted by the laminar theory, if turbulence has not occurred. But the data from these two samples does not lie near the theoretical line, but lies above it. This might indicate, then, that the flow is not laminar, but is turbulent. So with this thought in mind, a look at line 1 in Figure 25 shows that it does lie above the laminar theory line, but its slope is steep - steeper than that of the laminar theory line. This is very confusing because no data or theory is known to exist that predicts this sort of behavior.

Continuing with the other Samples 3 and 4, both are nylon ropes characterized by the same roughness ratio. But as was pointed out earlier, their surface appearances differ. Looking at lines 2 and 3 in Figure 25, both lie above the laminar theory line with shallower slopes. Their slopes are not quite equal, but the lines are fairly close together. In a qualitative way, Sample 4 (line 3) seems rougher in surface texture which might justify the larger drag coefficients characterized by line 3. But it is probably better to review Figures 22, 23, and 24 before coming to any hasty conclusions.

Figure 22 shows all of the data points together, and it is important to note the relationship between the Sample 3 and 4 data points. They really lie very close together. Adding the two Sample 3 points that created line 2 to the Sample 4 data points would not change line 3 much at all. Also, as

line 2 was drawn through only two data points it is statistically rather insignificant. Another very interesting observation can be made while looking at Figures 23 and 24. Only the circled data points were used to draw lines 2 and 3. One Sample 3 data point and seven Sample 4 data points were ignored to draw the lines. With transition and turbulence in mind, for Sample 4 especially, there could be a transition phenomenon occurring via those points. And line 3 bears the proper relationship to the laminar theory line to be a turbulent and/or roughness dominated line.

Without a lot more data over a larger range of Reynolds numbers and cable roughness or some theoretical predictions, it is very difficult to make quantitative conclusions from the data. If transition occurs outside of the Reynolds number range investigated here, for instance, the phenomenon would not be noticed. It seems safe to say that, with experimental error taken into account, all of the data points lie well above the laminar theory line. As there has been no theoretical analysis speaking to the problem of turbulent flow or the effects of cable roughness, it is not possible to conclude that turbulence and/or roughness effects have definitely caused this phenomenon. But based on other types of flow fields, similar results are the manifestation of turbulence and/or roughness. As some sort of transition phenomenon seems to occur for the nylon samples at a Reynolds number of about 10^5, the ballpark figure for transition near flat plates, there may be one more reason to feel that turbulence does occur near a tangentially oscillating cylinder. The wire rope data is puzzling as it does not lie near the laminar flow line nor slope in a way that characterizes either turbulence or roughness effects for other flowfields. Within the Sample 2 and 5 error bars, it would be possible to give line 1 a much shallower slope that would perhaps be more understandable. But as the choice of slope and

position for the line would be purely arbitrary, such a line would be of marginal use.

V. CONCLUSIONS

In summary, an experimental investigation of the tangential drag of an axially oscillating cylinder has been performed. Deep-sea mooring cables were oscillated sinusoidally at frequencies and amplitudes characteristic of ocean waves. The experimental data gives values of the tangential drag force and drag coefficient that are consistently higher than those values predicted by the laminar theory resulting from an exact solution to the Navier-Stokes equations. Cable roughness and turbulence effects are considered as reasons for the high-valued data. Without theoretical descriptions of turbulence and/or roughness effects, or a lot of experimental data, it is difficult to predict the exact relationship between the tangential drag coefficient and a rough cable and/or a turbulent flowfield.

Based on the experimental results, it is possible to make several recommendations for future work on the tangential drag of an axially oscillating cylinder. First, more experimental investigation is needed. It has been shown that meaningful values of the tangential drag forces and coefficients can be obtained even though the drag force is a small quantity compared to other forces in the system. As the values of the drag force and coefficient are consistently larger than the theoretical predictions, investigations of the specific effects of cable roughness and turbulence on the drag coefficient must be made. Or if any other effect could cause larger forces, it, too, should be investigated. A much larger range of Reynolds numbers must be included in future investigations, allowing both localized phenomena and general trends to be better understood. In the case of turbulence, it must first be determined if and when turbulence does occur. In future experiments, the drag force must be measured while studying

the boundary layer very closely; i.e., watching for turbulence, measuring boundary layer thicknesses, etc. And in all investigations, the experimental error must be as low as possible in order to pinpoint values more closely.

The experimental data indicated that the laminar theory is not predicting all of the observed drag force, so a more adequate theoretical description of the problem is needed. It would be very helpful to use a stability analysis of the problem in data interpretation; one could determine whether or not turbulence might occur using stability theory. No theory would include roughness factors unless it were based on experimental data, but in conjunction with more experimental data, such a theory could be developed.

In conclusion, much remains to be learned about the tangential drag of an axially oscillating cylinder. These experiments have served two purposes; they have produced some values of the tangential drag coefficient for real mooring cables and they have indicated that laminar theory alone is not adequate for predicting the observed drag forces. In short, more experimental and theoretical work must be done to fully understand the problem.

BIBLIOGRAPHY

1. Abramowitz, M. and Stegun, I.; Handbook of Mathematical Functions, Dover Publications, Inc., 1968.

2. Batchelor, G.K.; An Introduction to Fluid Dynamics, Cambridge University Press, 1970.

3. Berteaux, H.O., and Chhabra, N.; "Computer Programs for the Static Analysis of Single Point Moored Surface and Subsurface Buoy Systems", Woods Hole Oceanographic Institution Technical Report, March, 1973.

4. Carslaw, H.S. and Jaeger, J.C.; Conduction of Heat in Solids, Oxford University Press, 1959.

5. Casarella, M.J. and Laura, P.A.; "Drag on an Oscillating Rod with Longitudinal and Torsional Motion", Journal of Hydronautics, Vol. 3, #4, 1969.

6. Chandrasekhar, S.; Hydrodynamic and Hydromagnetic Stability, Oxford University Press, 1961.

7. Crandall, S.H., editor, et al; Random Vibrations Vol. II, Massachusetts Institute of Technology Press, 1963.

8. Goeller, J.E. and Laura, P.A.; "Analytical and Experimental Study of the Dynamic Response of Segmented Cable Systems", Journal of Sound and Vibration, 18(3), 1971.

9. Goldstein, S.; Modern Developments in Fluid Dynamics Vol. I & II, Dover Publications, Inc., 1965.

10. Goodman, T.R. et al; "Static and Dynamic Analysis of a Moored Buoy System", NOAA National Data Buoy Center, Report NDBCM 6113.1, April, 1972.

11. Gould, W.J. and Sambuco, E.; "The effect of mooring type on measured values of ocean currents", Deep-Sea Research, Vol. 22, 1975.

12. Grosch, C.E. and Salwen, H.; "The stability of Poiseuille flow in a pipe of circular cross-section", Journal of Fluid Mechanics, Vol. 54, 1972.

13. Hildebrand, F.B.; Advanced Calculus for Applications, Prentice-Hall, Inc., 1962.

14. Hoerner, S.F.; Fluid Dynamic Drag, published by the author, 1965.

15. Hong, S.-T.; "Frequency Domain Analysis for the Tension in a Taut-Mooring Line", Department of Civil Engineering, University of Washington, Technical Report No. SM72-1, July, 1972.

16. Kaplan, P. et al; "Experimental and Analytical Studies of Buoy Hull Motions in Waves", NOAA National Data Buoy Center, Report NDBC 6113.3, April, 1972.

17. Landau, L.D. and Lifschitz, E.M.; Fluid Mechanics, Addison-Wesley, 1959.

18. Myers, J.J., editor, et al; Handbook of Ocean and Underwater Engineering, McGraw-Hill Book Co., 1969.

19. Newman, J.N.; Marine Hydrodynamics, lecture notes, Massachusetts Institute of Technology, revised edition, Spring Term 1971.

20. Obremski, H.J. et al; "A Portfolio of Stability Characteristics of Incompressible Boundary Layers", NATO, AGARDograph 134, March, 1969.

21. Orszag, S.A.; personal communication, June, 1975.

22. Panicker, N.N., Susan Schultz Tapscott, et al; "Analysis of Surface Mooring Dynamics", Offshore Technology Conference, paper number OTC 2071, 1974.

23. Roark, R.J.; Formulas for Stress and Strain, McGraw-Hill Book Co., 1965.

24. Sargent, T.P. et al; "Computer Program Documentation Report: Buoy-Cable Dynamics Program", NOAA National Data Buoy Center, Report NDBC 6113.2, April, 1972.

25. Schlichting, H., Boundary-Layer Theory, McGraw-Hill Book Co., 1968.

26. Shigley, J.E.; Mechanical Engineering Design, McGraw-Hill Book Co., 1963.

27. Stokes, G.G.; Mathematical and Physical Papers Vol. III, Cambridge University Press, 1901.

28. Taussig, R.; "Motions of a Spar Raft in Regular Waves", Department of the Navy, David Taylor Model Basin, Hydromechanics Laboratory, Research and Development Report #1673, May, 1963.

29. Walden, R.G. and Panicker, N.N.; "Performance Analysis of Woods Hole Taut Moorings", Woods Hole Oceanographic Institution, Technical Report W.H.O.I. 73-31, June, 1973.

30. Yamamoto, T. et al; "Longitudinal motions of taut moorings", The American Society of Civil Engineers, Waterways, Harbors and Coastal Engineering Journal, Proceedings of the ASCE, Vol. 82, WW1, February, 1974.

TITLES OF TABLES

TABLE 1

Test Sample Specifications

Sample Number	Material	lay	diameter (in.)	ρ rope density (slugs/ft^3)	dry weight / ft. (lb./ft.)	wet weight / ft. (lb./ft.)	q roughness ratio (in./in.)	Additional Description
2	wire	3x19 TB +	.392	5.59×10^{-3}	.179	.121	.020	smooth, poly-ethylene jacket covering wire strands
3	nylon	plaited	.750	4.53×10^{-3}	.145	.100	.100	many irregular bumps on rope surface, small strands of rope for plaiting
4	nylon	3 strand	1.00	8.12×10^{-3}	.260	.022	.098	large rope strands twisted in ordered fashion
5	wire	3x19 TB +	.456	7.91×10^{-3}	.253	.175	.020	smooth, poly-ethylene jacket covering wire strands

* in fresh water + TB = torque balanced

TABLE 2

Fresh Water Properties *

T (°C)	ρ (slugs/ft.^{3})	μ 10^5 (slugs/ft.-s)	ν x 10^5 (ft.^{2}/s)
12.0	1.942	2.544	1.310
20.0	1.938	2.074	1.070
22.0	1.937	1.950	1.007
24.5	1.934	1.837	.950

* (Myers et al, 1969)

TABLE 3

Data

3-1 Test 1
Sample 2 - polyethylene jacketed wire rope
a = .0165 ft.
water temperature 12° C
oscillation amplitude A = 30 cm. = .984 ft.

A	T(s)	ω(rad/s)	F_T data	F_T predict	C_T data	C_T predict	Re_A x10^{-5}	f(aα)	Re_a	C_TA/d data	S/N	avg. # data cycles
A	4.5	1.396	.094	.026	.0240	.0066	1.03	1.067	29.01	.7079	.030	17
	2.8	2.244	.130	.052	.0130	.0052	1.66	1.052	46.64	.3834	.032	22

3-2 Test 2
Sample 3 - plaited nylon
a = .0312 ft.
water temperature 12° C
oscillation amplitude A = 46 cm. = 1.509 ft.

A	T(s)	ω(rad/s)	F_T data	F_T predict	C_T data	C_T predict	Re_A x 10^{-5}	f(aα)	Re_a	C_TA/d data	S/N	avg. # data cycles
A	4.5	1.396	.106	.073	.0061	.0042	2.43	1.035	103.7	.2950	.033	13
	3.6	1.745	.236	.102	.0087	.0037	3.03	1.031	129.7	.4208	.060	15
	2.8	2.244	.378	.148	.0084	.0033	3.90	1.027	166.7	.4063	.074	24

3-3 Test 3
Sample 4 - 3-strand nylon
a = .0415 ft.
water temperature 12° C
oscillation amplitudes A_1 = 42 cm. = 1.3776 ft., A_2 = 30 cm. = .984 ft.

A	T(s)	ω(rad/s)	F_T data	F_T predict	C_T data	C_T predict	$Re_A \times 10^{-5}$	f(aα)	Re_a	$C_T A/d$ data	S/N	avg. # data cycles
A_1	4.5	1.396	.118	.088	.0060	.0046	2.02	1.026	183.5	.1001	.020	11
	3.6	1.745	.402	.123	.0132	.0041	2.53	1.023	229.4	.220	.061	15
	2.8	2.244	.508	.179	.0101	.0036	3.25	1.021	295.0	.1675	.065	15
A_2	3.6	1.745	.224	.091	.0144	.0057	1.29	1.023	229.4	.1712	.038	15
	2.8	2.244	.472	.132	.0184	.0050	1.66	1.021	295.0	.2186	.069	20

3-4 Test 4
Sample 4 - 3-strand nylon
a = .0415 ft.
water temperature 20° C
oscillation amplitudes A_1 = 45 cm. = 1.476 ft., A_2 = 30 cm. = .984 ft.

A	T(s)	ω(rad/s)	F_T data	F_T predict	C_T data	C_T predict	$Re_A \times 10^{-5}$	f(aα)	Re_a	$C_T A/d$ data	S/N	avg # data cycles
A_1	4.5	1.396	.218	.089	.0097	.0038	2.84	1.024	224.7	.1732	.034	14
	3.6	1.745	.460	.124	.0132	.0034	3.55	1.021	280.9	.2346	.067	19
	2.8	2.244	.714	.180	.0124	.0030	4.57	1.019	361.2	.2206	.088	17

3-4 (con't)

A	T(s)	ω(rad/s)	F_T data	F_T predict	C_T data	C_T predict	$Re_A \times 10^{-5}$	f(aα)	Re_a	$C_T A/d$ data	S/N	avg. # data cycles
A_2	5.6	1.122	.094	.043	.0147	.0064	1.02	1.026	180.6	.1739	.016	12
	4.5	1.396	.154	.059	.0156	.0058	1.26	1.024	224.7	.1844	.025	16
	3.6	1.745	.260	.082	.0168	.0051	1.58	1.021	280.9	.1996	.040	21
	2.8	2.244	.408	.120	.0159	.0045	2.03	1.019	361.2	.1890	.055	24

3-5 Test 5
Sample 4 - 3-strand nylon
a = .0415 ft.
water temperature 22° C
oscillation amplitudes A_1 = 45 cm. = 1.476 ft., A_2 = 30 cm. = .984 ft.
middle water test; l_{h-1} = 20.75 ft., l_{h-m} = 10.66 ft., l_{m-1} = 10.10 ft.

A	1*	T(s)	ω(rad/s)	F_T data	F_T predict	C_T data	C_T predict	$Re_A \times 10^{-5}$	f(aα)	Re_a	$C_T A/d$ data	S/N	avg.# data cycles
A_1	l_{m-1}	2.8	2.244	.212	.076	.0087	.0032	4.229	1.018	383.8	.1547	.109	20
A_2	l_{m-1}	2.8	2.244	.142	.054	.0114	.0044	2.158	1.018	383.8	.1351	.101	23

* l denotes section of the test sample over which drag force was measured

3-6 Test 6
Sample 4 - 3-strand nylon
a = .0415 ft.
water temperature 24.5° C
oscillation amplitude: A = 30 cm. = .984 ft.
middle water test; l_{h-l} = 20.75 ft. , l_{h-m} = 10.66 ft., l_{m-l} = 10.10 ft.

A	1*	T(s)	ω(rad/s)	F_T data	F_T predict	C_T data	C_T predict	$Re_A \times 10^{-5}$	f(aα)	Re_a	C_TA/d data	S/N	avg. # data cycles
A	l_{h-l}	5.6	1.122	.035	.038	.0055	.0061	1.144	1.025	203.4	.0652	.006	14
		4.5	1.396	.094	.053	.0095	.0054	1.423	1.022	253.1	.1126	.015	16
		3.6	1.745	.189	.074	.0122	.0048	1.778	1.020	316.4	.1446	.030	22
		2.8	2.244	.307	.108	.0120	.0042	2.287	1.018	406.8	.1423	.045	31
	l_{h-m}	5.6	1.122	.024	.020	.0073	.0061	1.144	1.025	203.4	.0865	.006	14
		4.5	1.396	.059	.027	.0116	.0054	1.423	1.022	253.1	.1375	.015	16
		3.6	1.745	.094	.038	.0119	.0048	1.778	1.020	316.4	.1411	.030	22
		2.8	2.244	.165	.055	.0126	.0042	2.287	1.018	406.8	.1494	.045	31
	l_{m-l}	5.6	1.122	.012	.019	.0039	.0061	1.144	1.025	203.4	.0462	.006	14
		4.5	1.396	.035	.026	.0073	.0054	1.423	1.022	253.1	.0865	.015	16
		3.6	1.745	.094	.036	.0125	.0048	1.778	1.020	316.4	.1482	.030	22
		2.8	2.244	.142	.052	.0114	.0042	2.287	1.018	406.8	.1352	.045	31

*1 denotes section of test sample over which drag force was measured

3-7 Test 7
Sample 5 - polyethylene jacketed wire rope
a = .019 ft.
water temperature 20° C
oscillation amplitudes A_1 = 45 cm. = 1.476 ft., A_2 = 30 cm. = .984 ft.

A	T(s)	ω(rad/s)	F_T data	F_T predict	C_T data	C_T predict	$Re_A \times 10^{-5}$	f(aα)	Re_a	$C_T A/d$ data	S/N	avg. # data cycles
A_1	5.6	1.122	.083	.030	.0126	.0044	2.28	1.058	37.85	.4895	.013	9
	4.5	1.396	.100	.042	.0098	.0040	2.84	1.052	47.10	.3824	.015	12
A_2	2.8	2.244	.177	.056	.0152	.0046	2.03	1.041	75.71	.3926	.026	21

TABLE 4

Needle Frequency Comparison

Test Number	Water Level	A (cm)	T (s)	Observed Frequency (c/s)	Observed Frequency (c/s)	
					n_a	n_i
2	high	46	18.5	2.0	1.7	
			12.0	6.5	2.6	
			6.1	6.0	5.0	
			4.5	6.75	6.8	
			3.6	8.0		8.5
			2.8	6.4		6.4
3	high	30	18.5	1.5	1.1	
			12.0	2.0	1.7	
			6.1	3.5	3.3	
			4.5	5.0	4.4	
			3.6	5.7		5.6
			2.8	5.0		4.2
4	high	45	18.5	2.0	1.6	
			5.6	5.5	5.4	
			4.5	6.0	6.7	
			3.6	7.0		6.7
			2.8	6.0		6.5

TITLES OF FIGURES

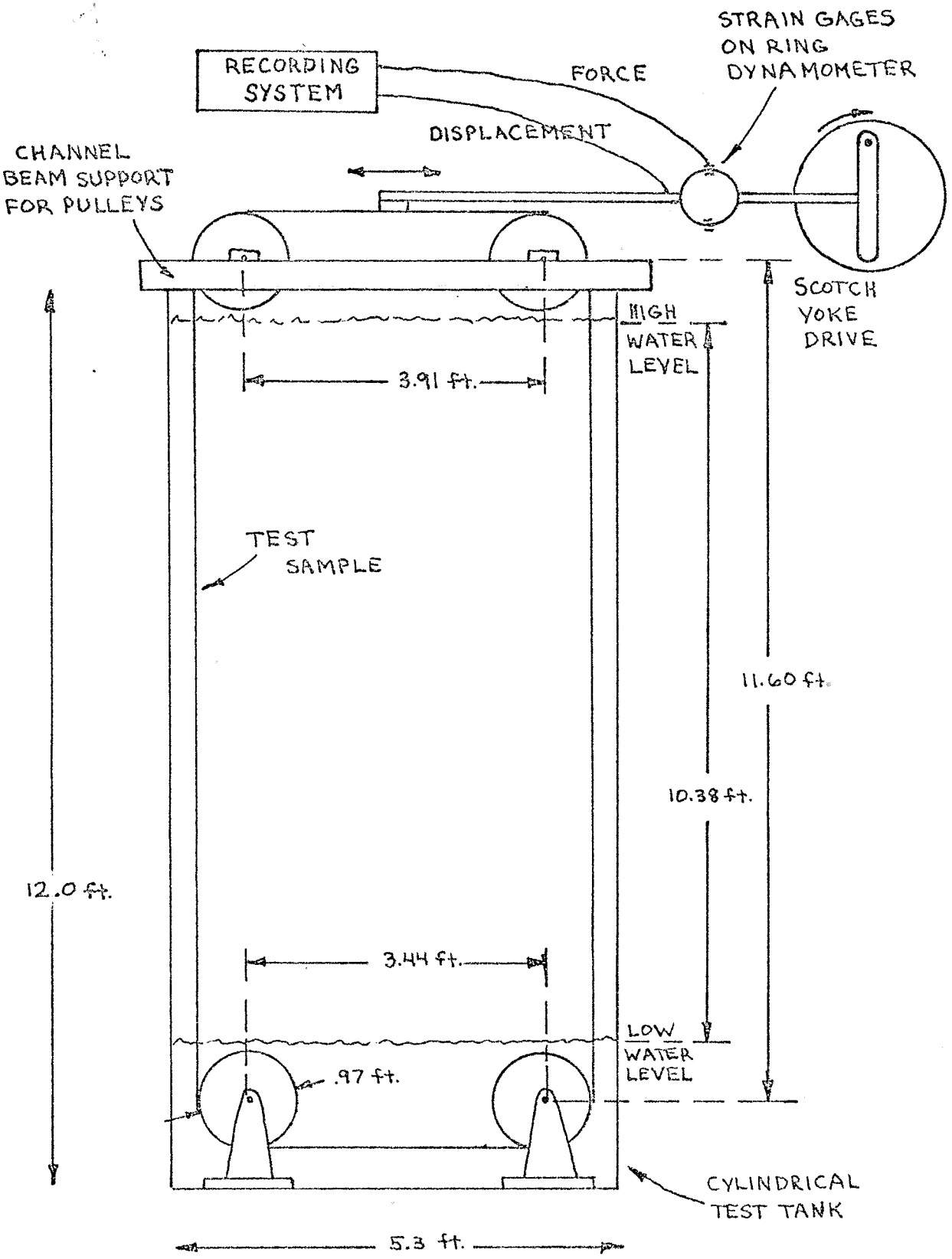
RECORDING SYSTEM
FORCE
DISPLACEMENT
STRAIN GAGES ON RING DYNAMOMETER
CHANNEL BEAM SUPPORT FOR PULLEYS
SCOTCH YOKE DRIVE
HIGH WATER LEVEL
3.91 ft.
TEST SAMPLE
11.60 ft.
10.38 ft.
12.0 ft.
3.44 ft.
LOW WATER LEVEL
.97 ft.
CYLINDRICAL TEST TANK
5.3 ft.

FIGURE 1

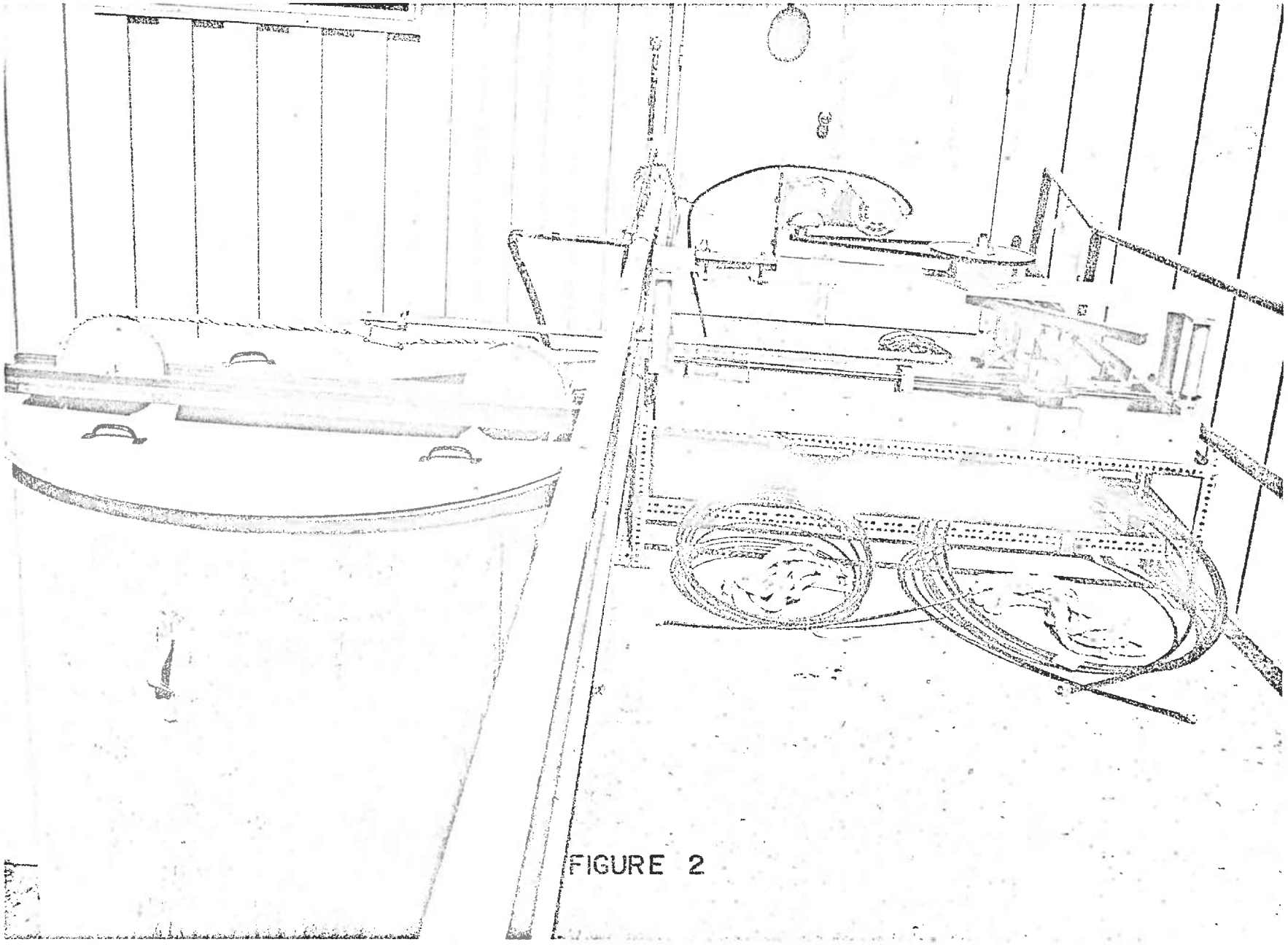

FIGURE 2

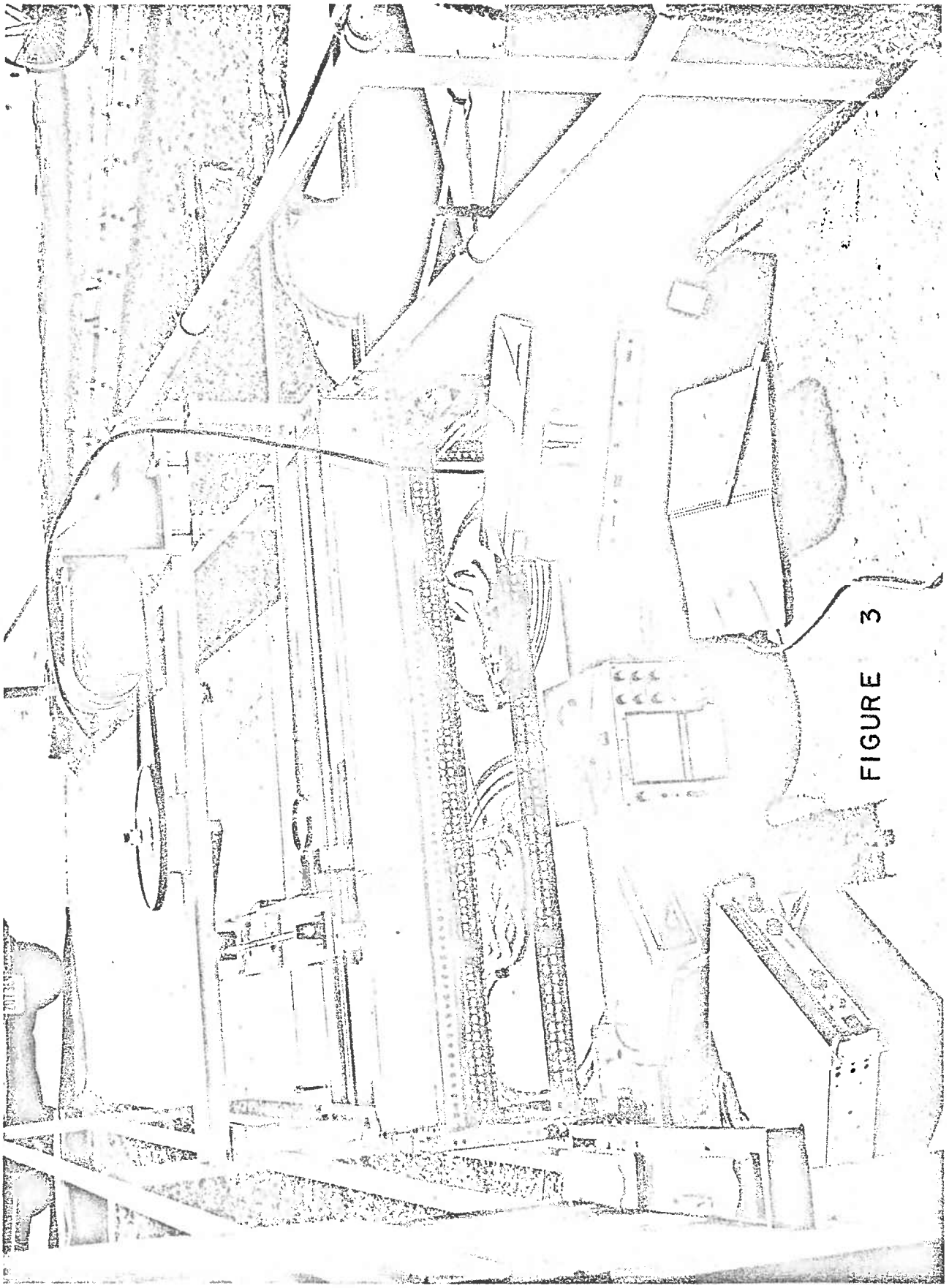

FIGURE 3

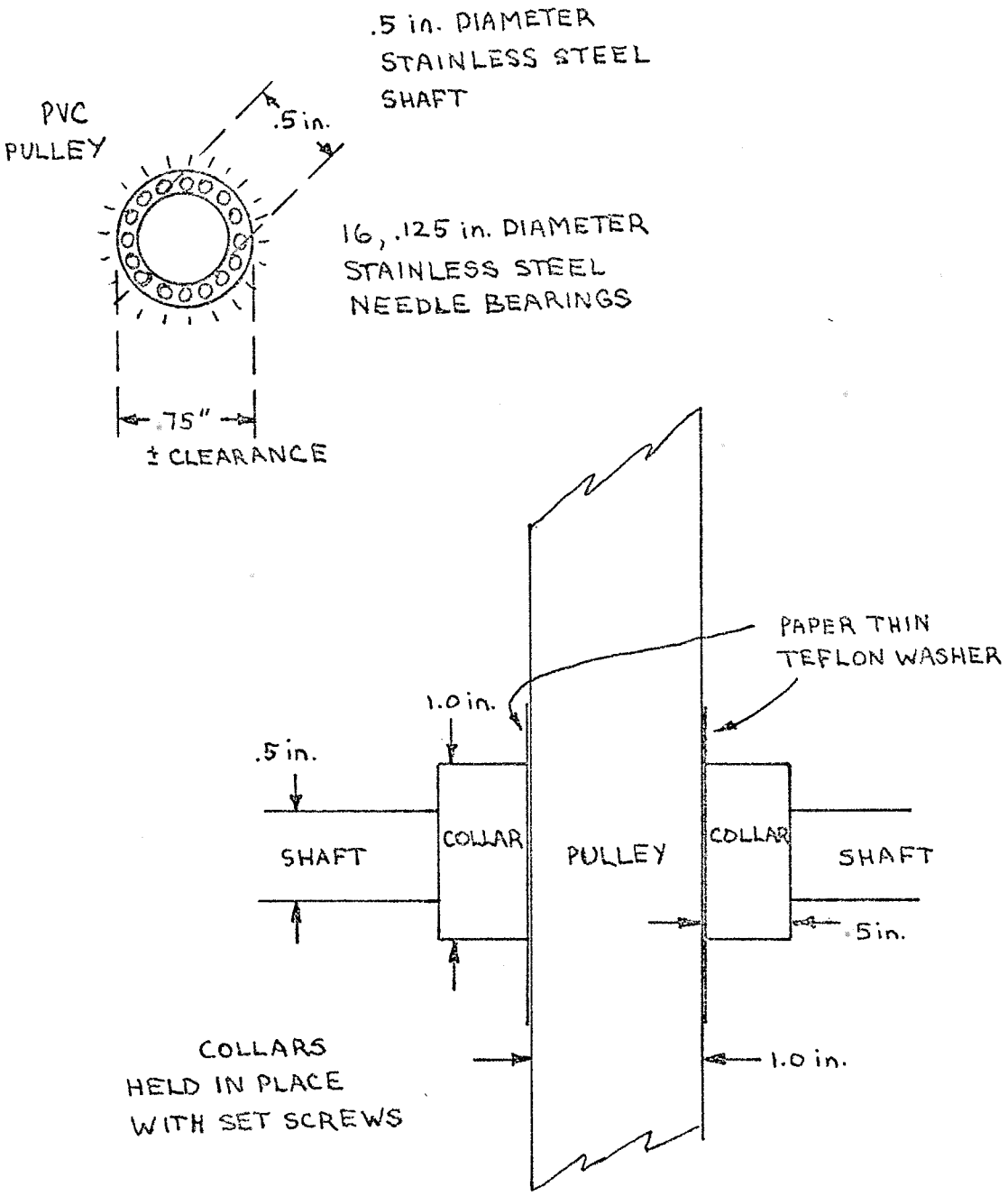
.5 in. DIAMETER
STAINLESS STEEL
SHAFT
PVC
PULLEY
.5 in.
16, .125 in. DIAMETER
STAINLESS STEEL
NEEDLE BEARINGS
.75"
± CLEARANCE
PAPER THIN
TEFLON WASHER
1.0 in.
.5 in.
SHAFT
COLLAR
PULLEY
COLLAR
SHAFT
.5in.
1.0 in.
COLLARS
HELD IN PLACE
WITH SET SCREWS

FIGURE 4

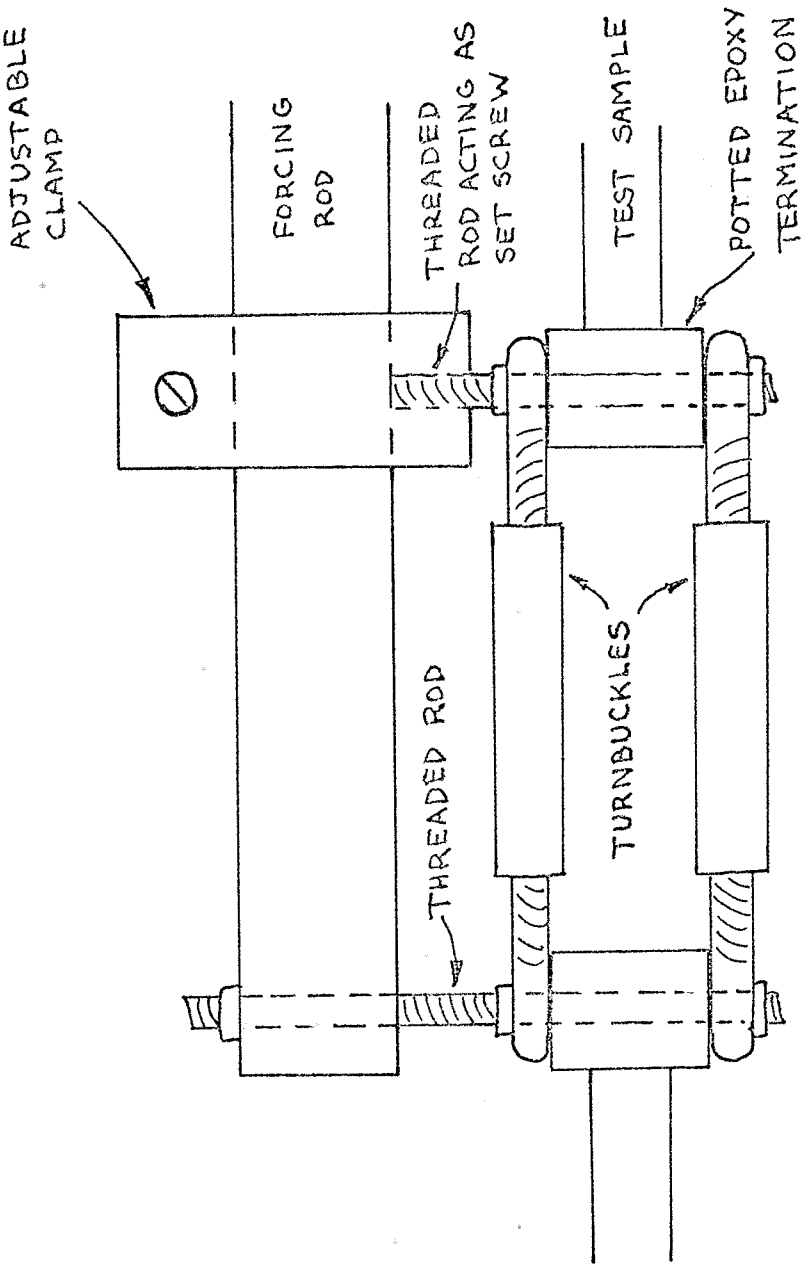
ADJUSTABLE CLAMP
FORCING ROD
THREADED ROD ACTING AS SET SCREW
TEST SAMPLE
POTTED EPOXY TERMINATION
THREADED ROD
TURNBUCKLES

FIGURE 5

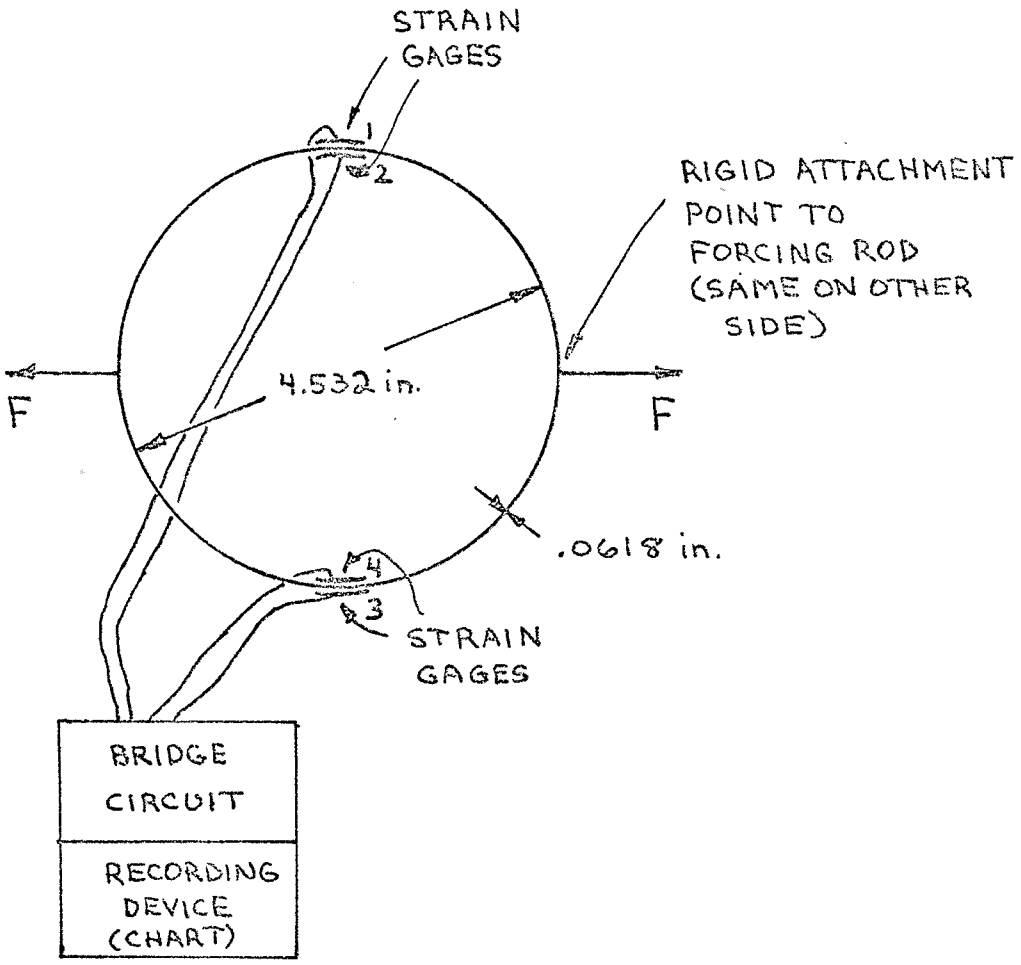
STRAIN
GAGES
1
2
RIGID ATTACHMENT
POINT TO
FORCING ROD
(SAME ON OTHER
SIDE)
4.532 in.
F
F
.0618 in.
4
3
STRAIN
GAGES
BRIDGE
CIRCUIT
RECORDING
DEVICE
(CHART)

FIGURE 6

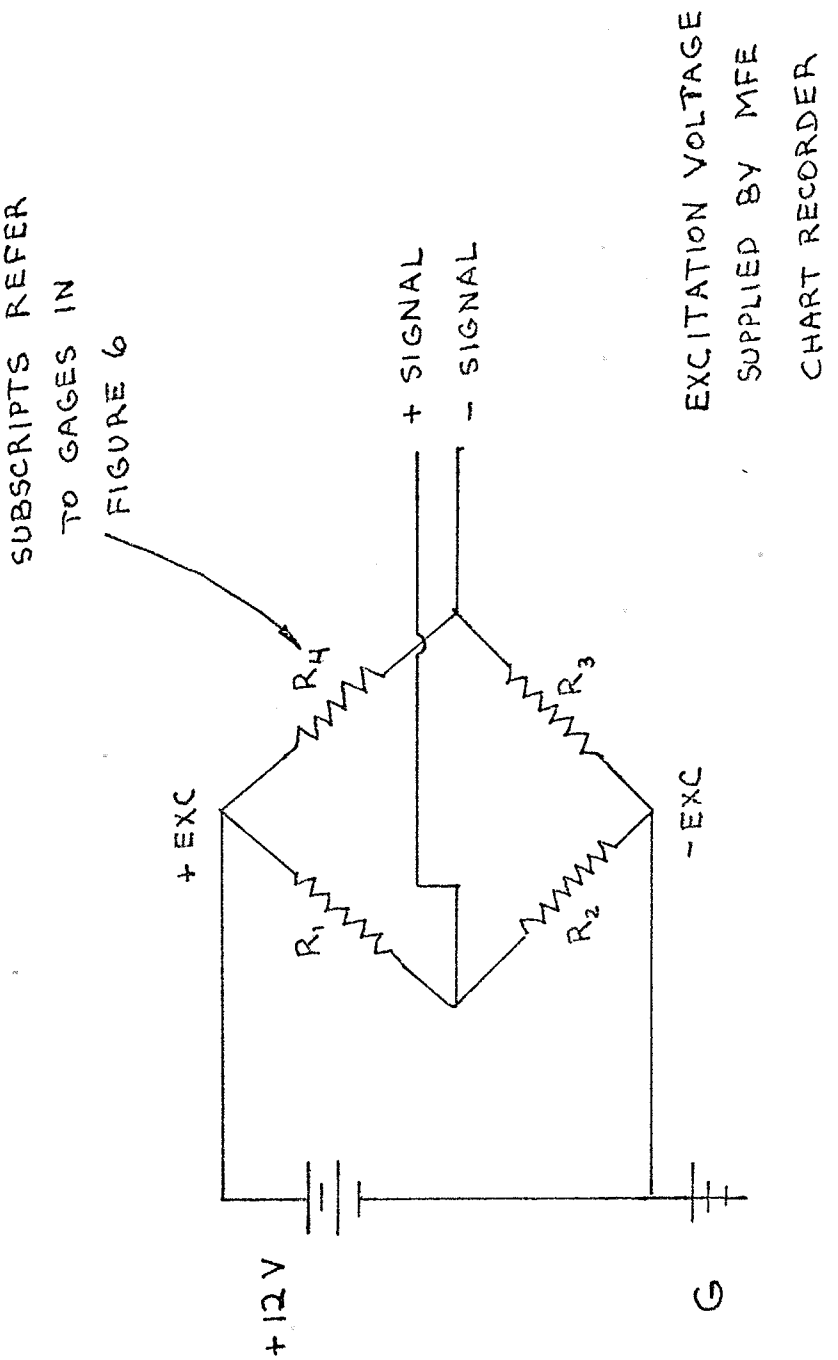
SUBSCRIPTS REFER
TO GAGES IN
FIGURE 6
+ SIGNAL
- SIGNAL
EXCITATION VOLTAGE
SUPPLIED BY MFE
CHART RECORDER
R_4
R_3
R_1
R_2
+ EXC
- EXC
+12 V
G

FIGURE 7

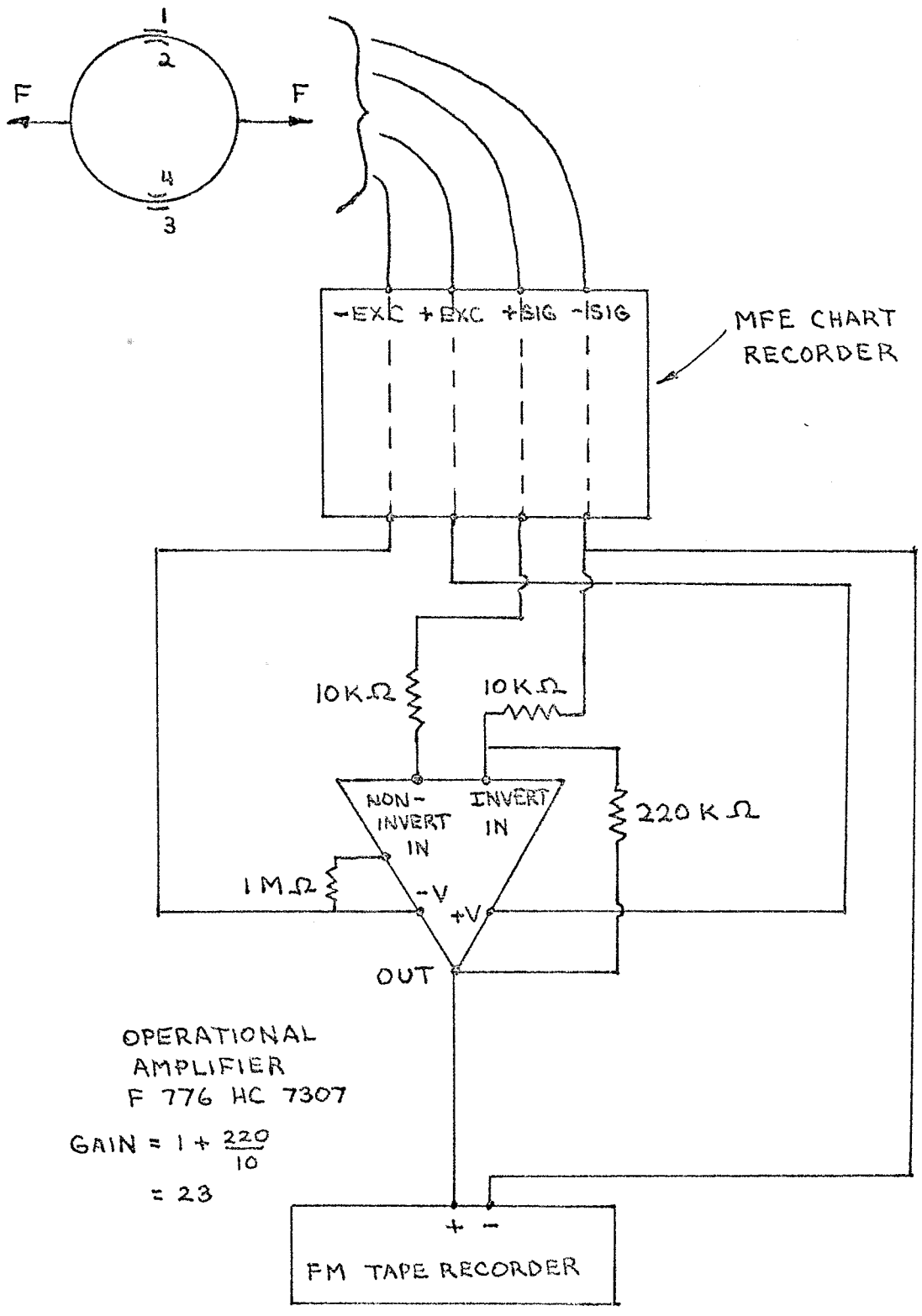
1
2
F
F
4
3
-EXC
+EXC
+SIG
-SIG
MFE CHART RECORDER
10KΩ
10KΩ
NON-INVERT IN
INVERT IN
220KΩ
1MΩ
-V
+V
OUT
OPERATIONAL AMPLIFIER
F 776 HC 7307
GAIN = 1 + 220/10
= 23
+
-
FM TAPE RECORDER

FIGURE 8

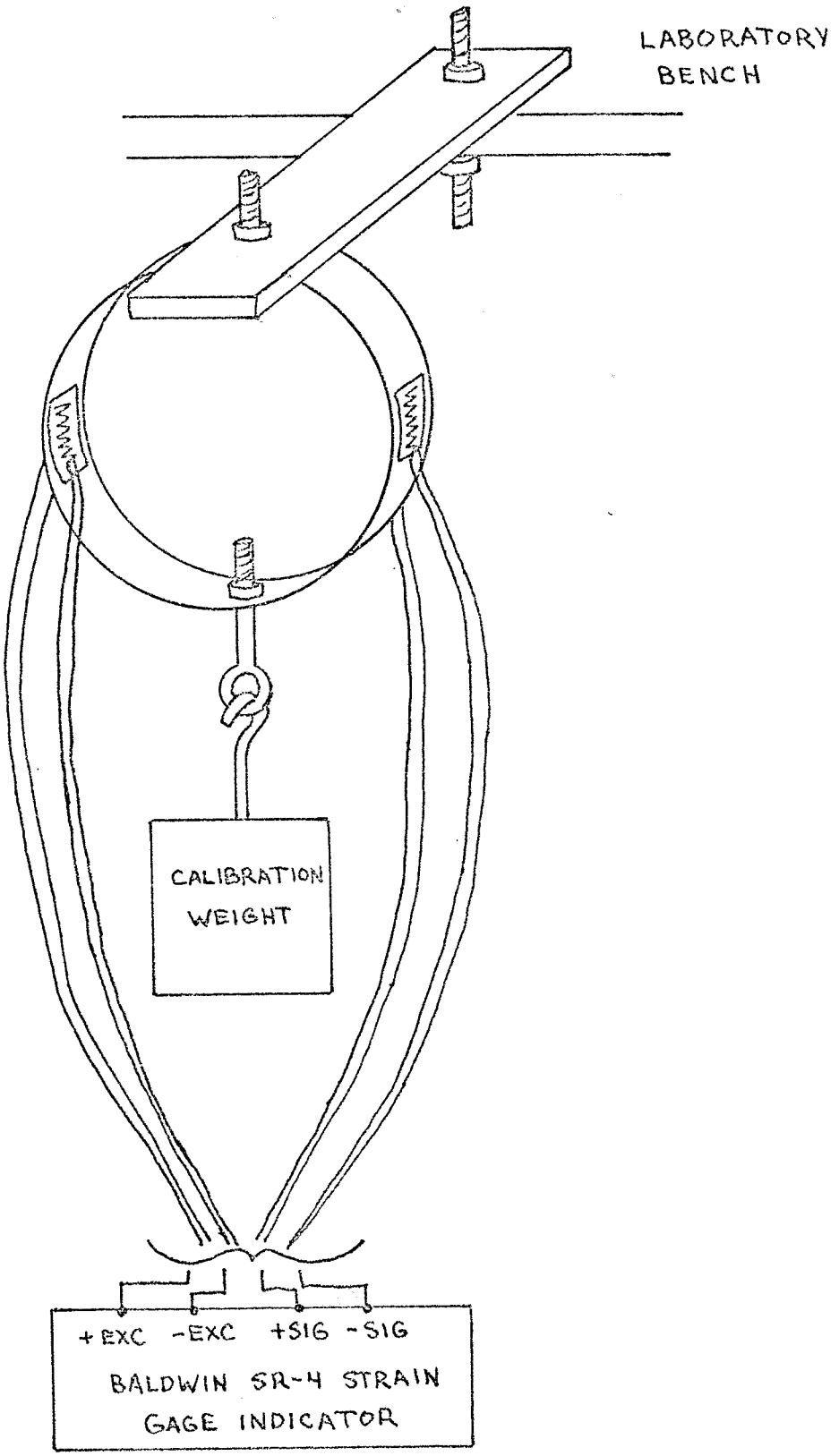
LABORATORY
BENCH
CALIBRATION
WEIGHT
+EXC -EXC +SIG -SIG
BALDWIN SR-4 STRAIN
GAGE INDICATOR

FIGURE 9

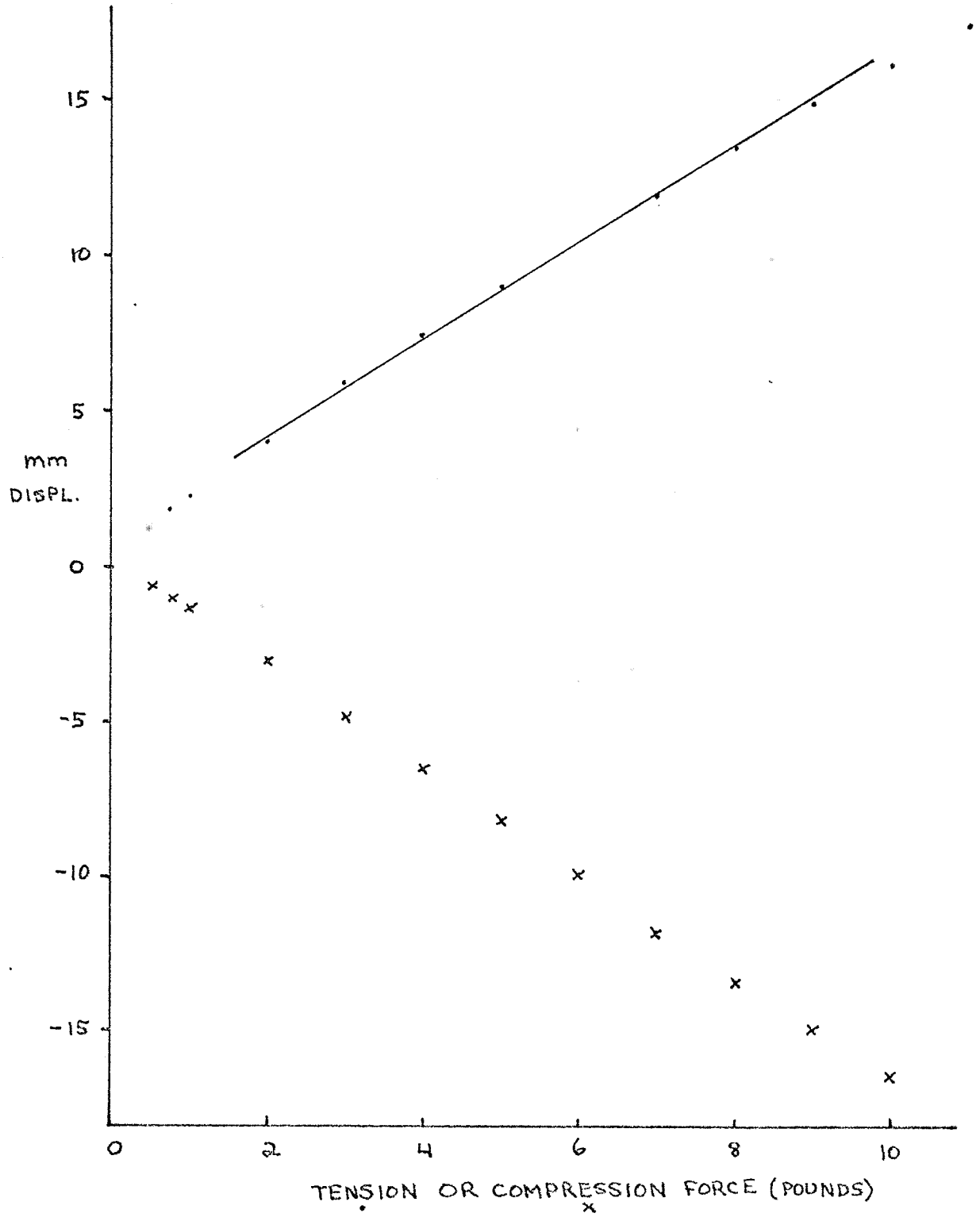
15
10
5
mm
DISPL.
0
-5
-10
-15
0
2
4
6
8
10
TENSION OR COMPRESSION FORCE (POUNDS)

FIGURE 10

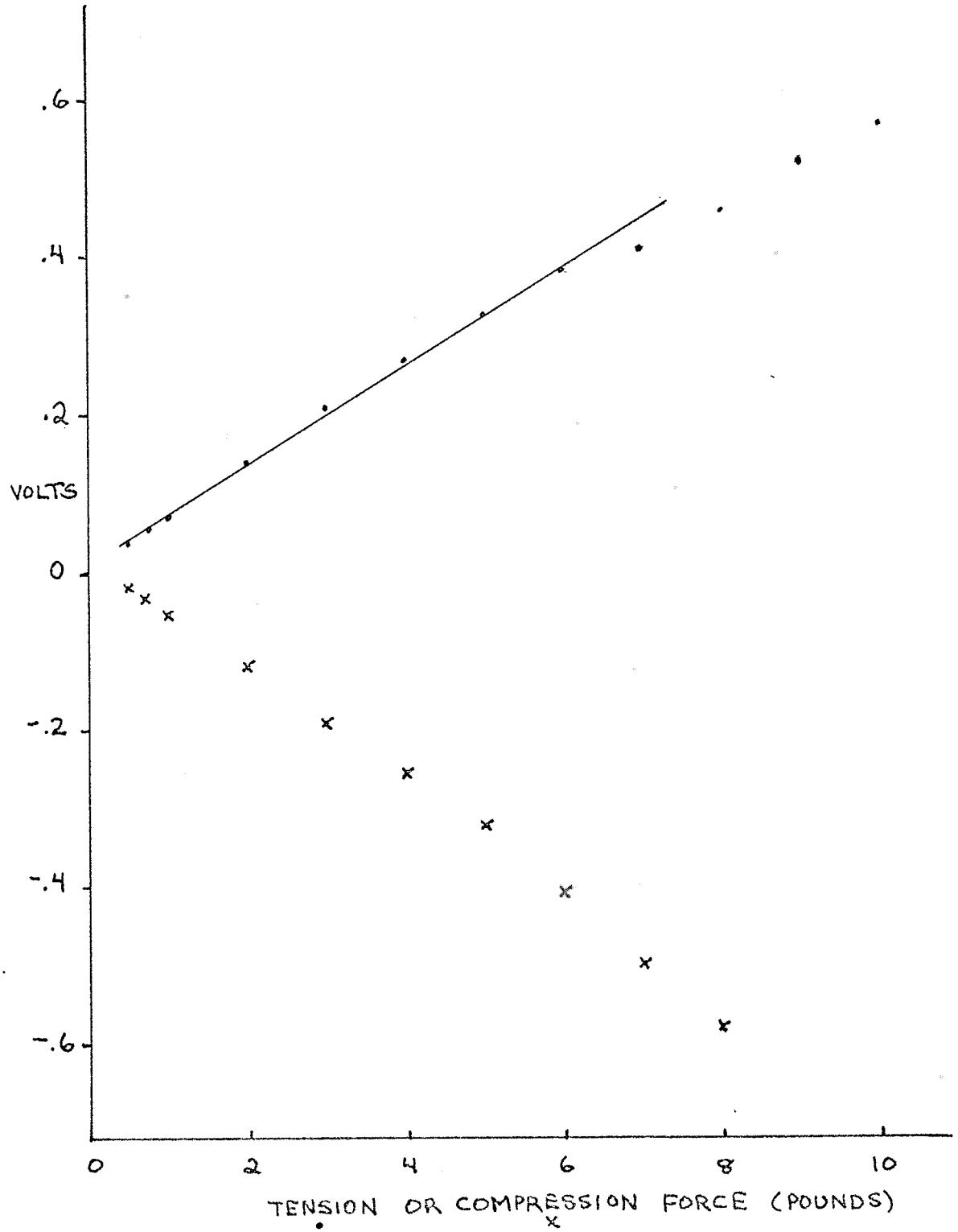
.6
.4
.2
VOLTS
0
-.2
-.4
-.6
0
2
4
6
8
10
TENSION OR COMPRESSION FORCE (POUNDS)

FIGURE 11

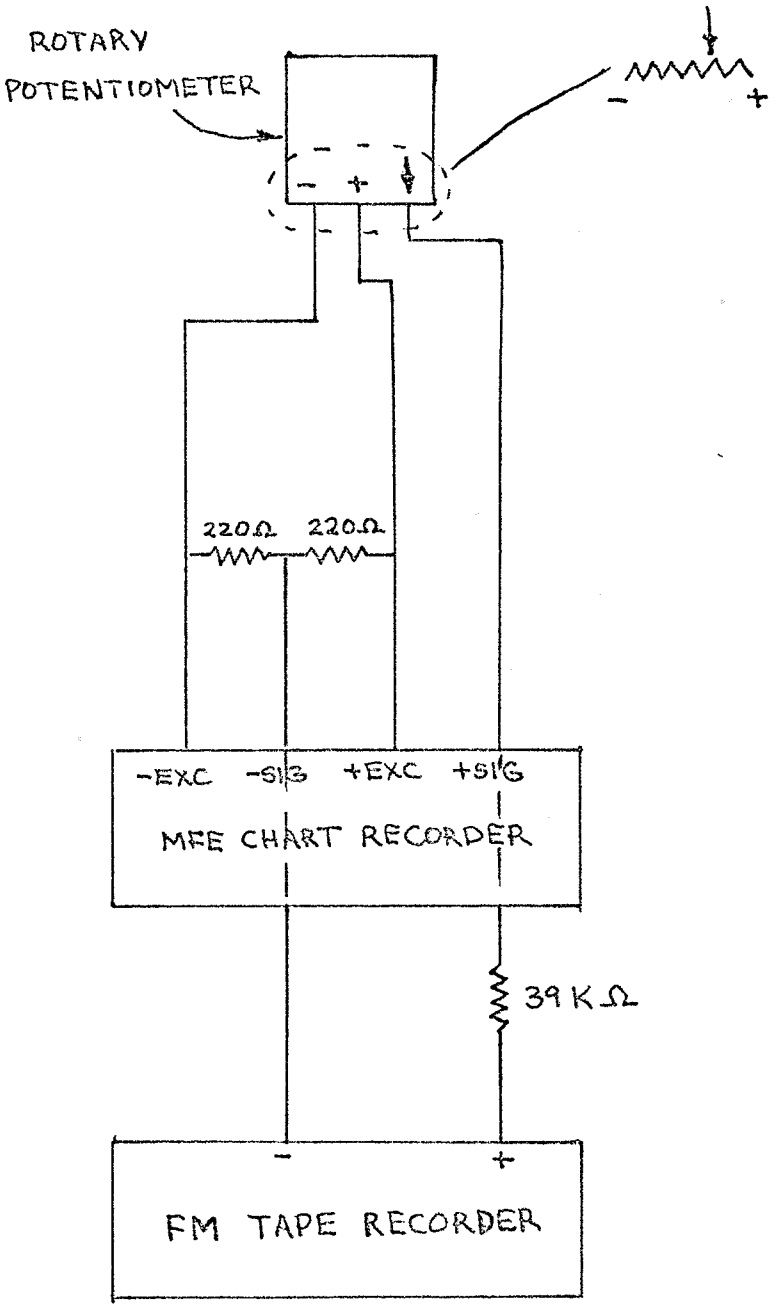
ROTARY
POTENTIOMETER
220Ω
220Ω
-EXC
-SIG
+EXC
+SIG
MFE CHART RECORDER
39 KΩ
FM TAPE RECORDER

FIGURE 12

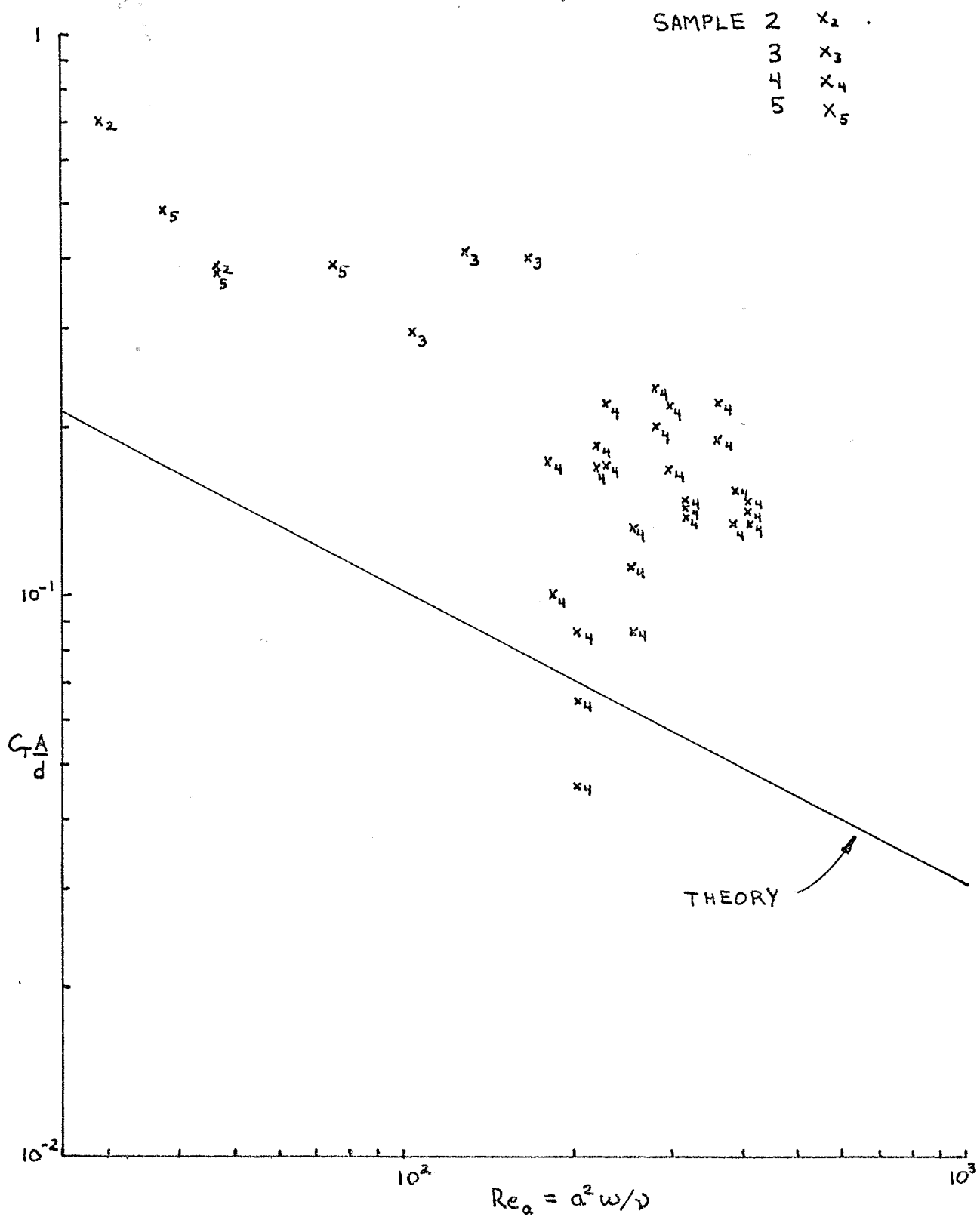

FIGURE 13

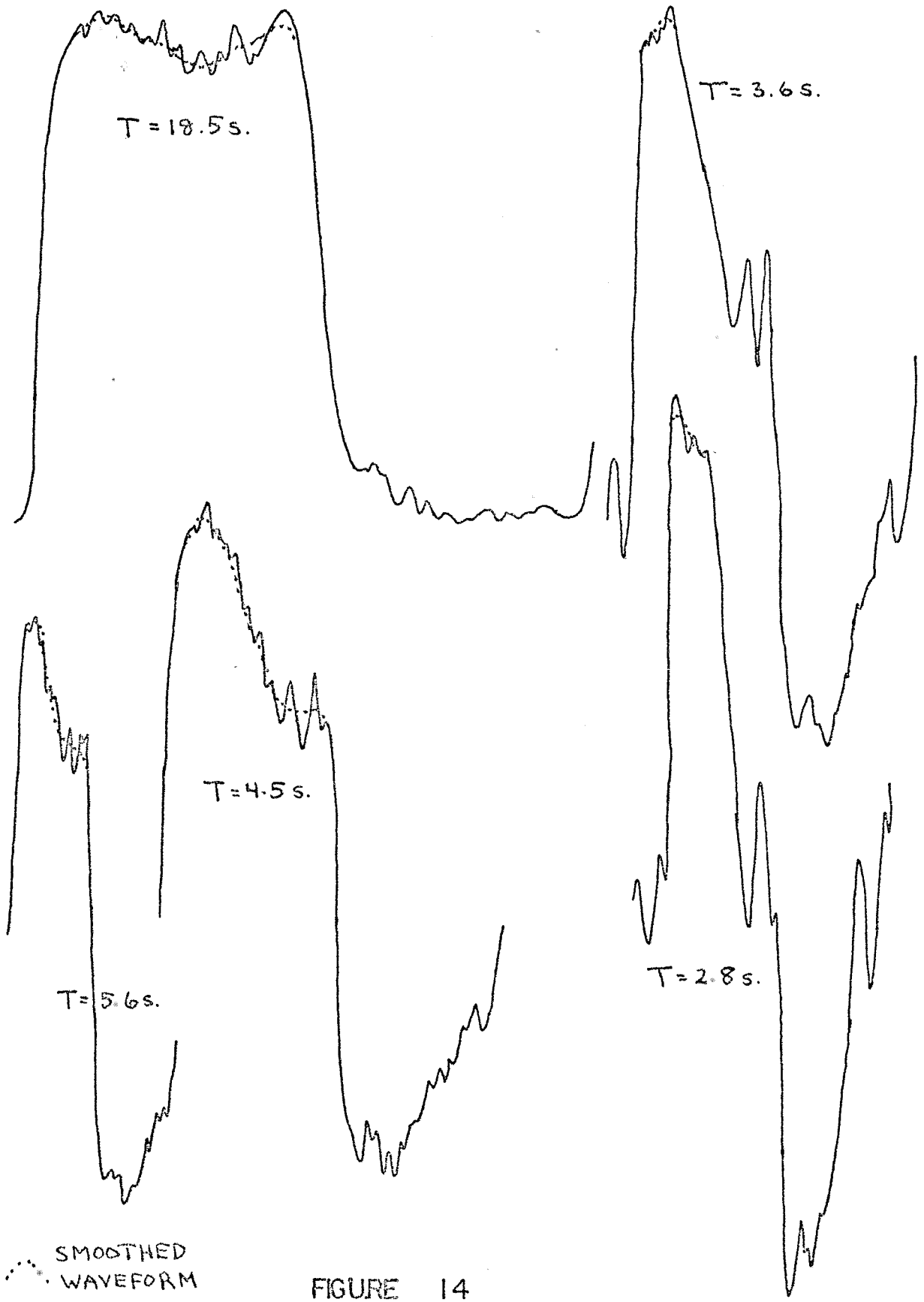

FIGURE 14

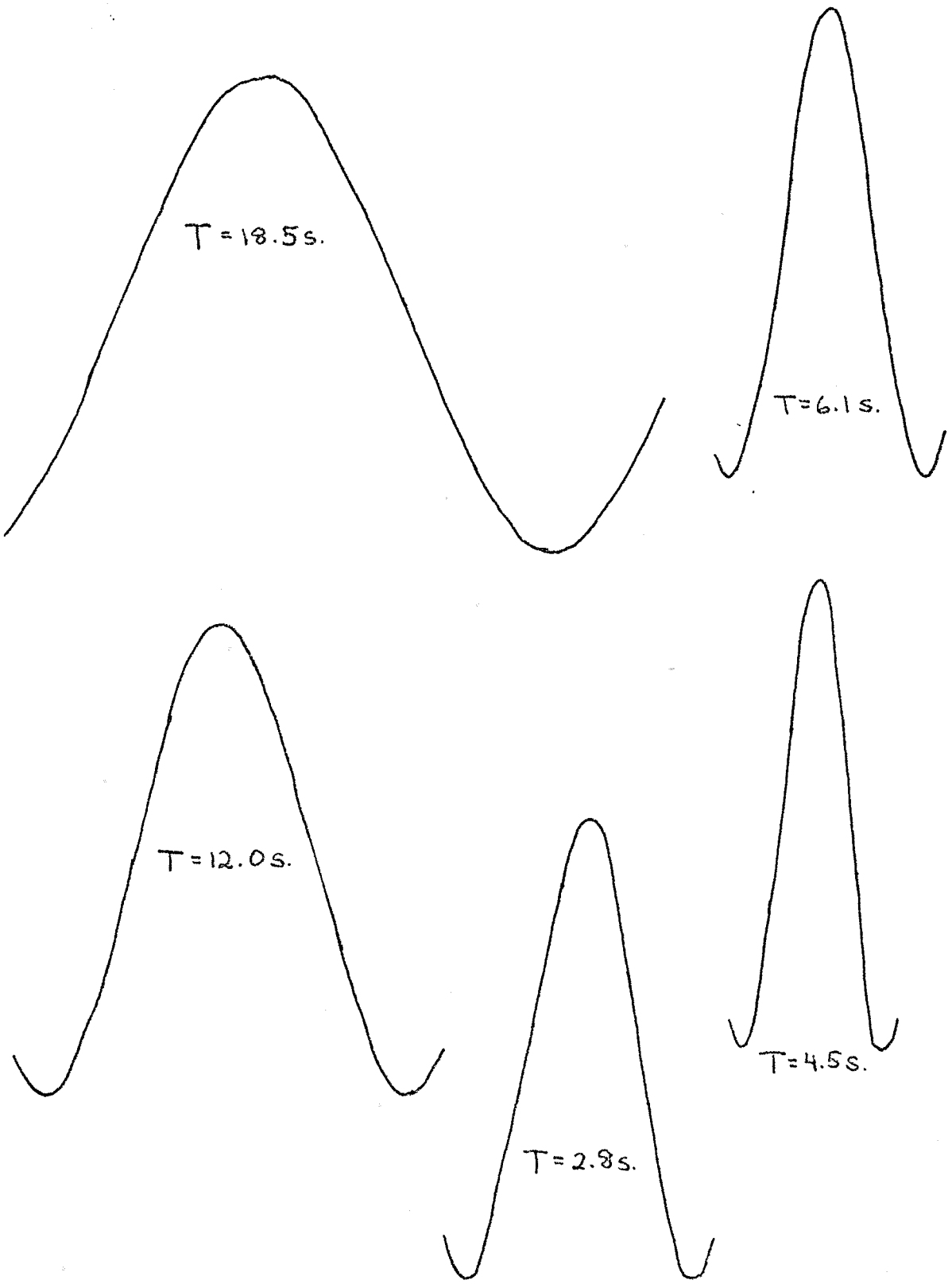

FIGURE 15

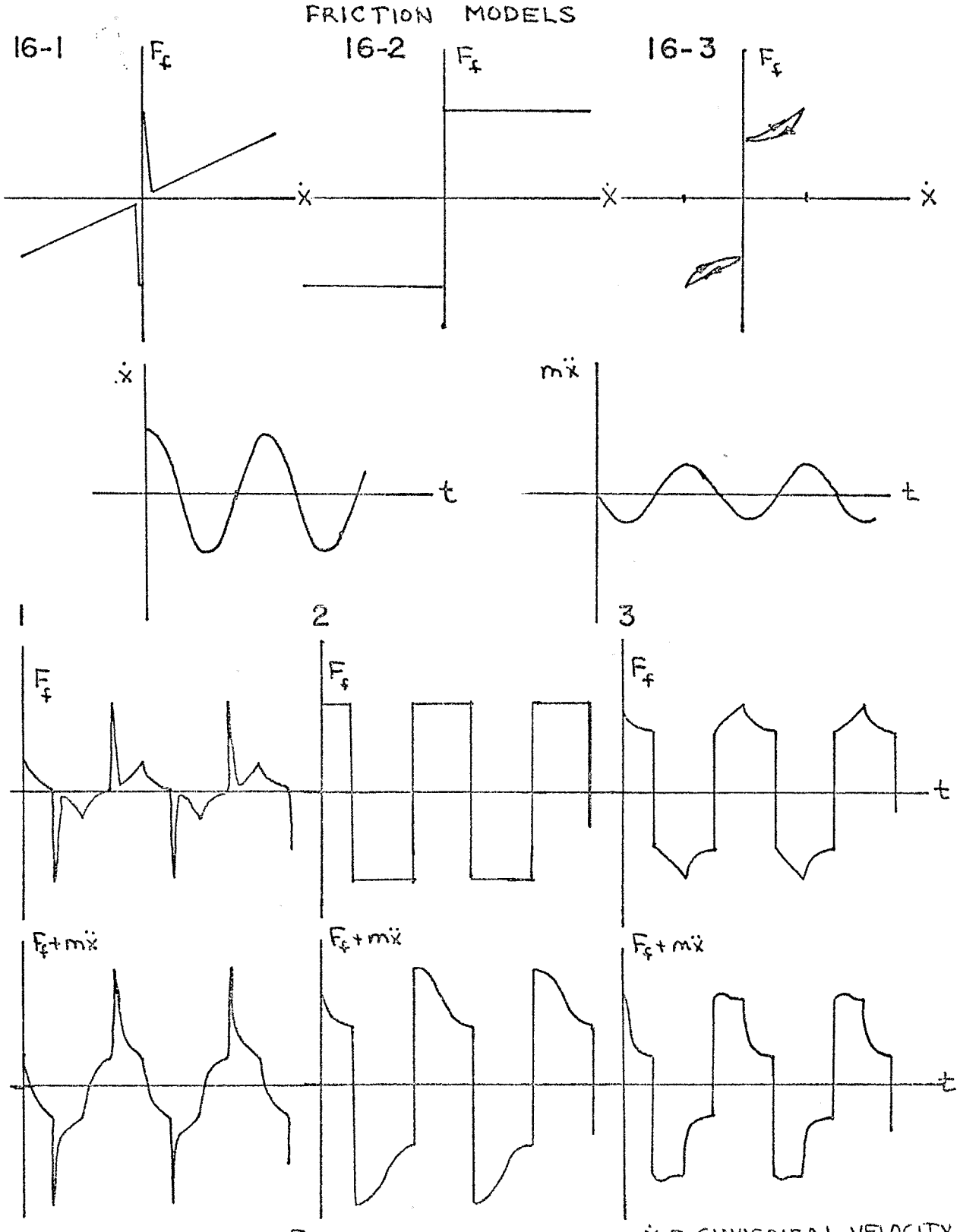
FRICTION MODELS
16-1
16-2
16-3
F_f
$\dot{x}$
$m\ddot{x}$
t
1
2
3
$F_f + m\ddot{x}$
F_f ≡ FRICTION FORCE
$\dot{x}$ ≡ SINUSOIDAL VELOCITY
$m\ddot{x}$ ≡ SINUSOIDAL INERTIAL FORCE

FIGURE 16

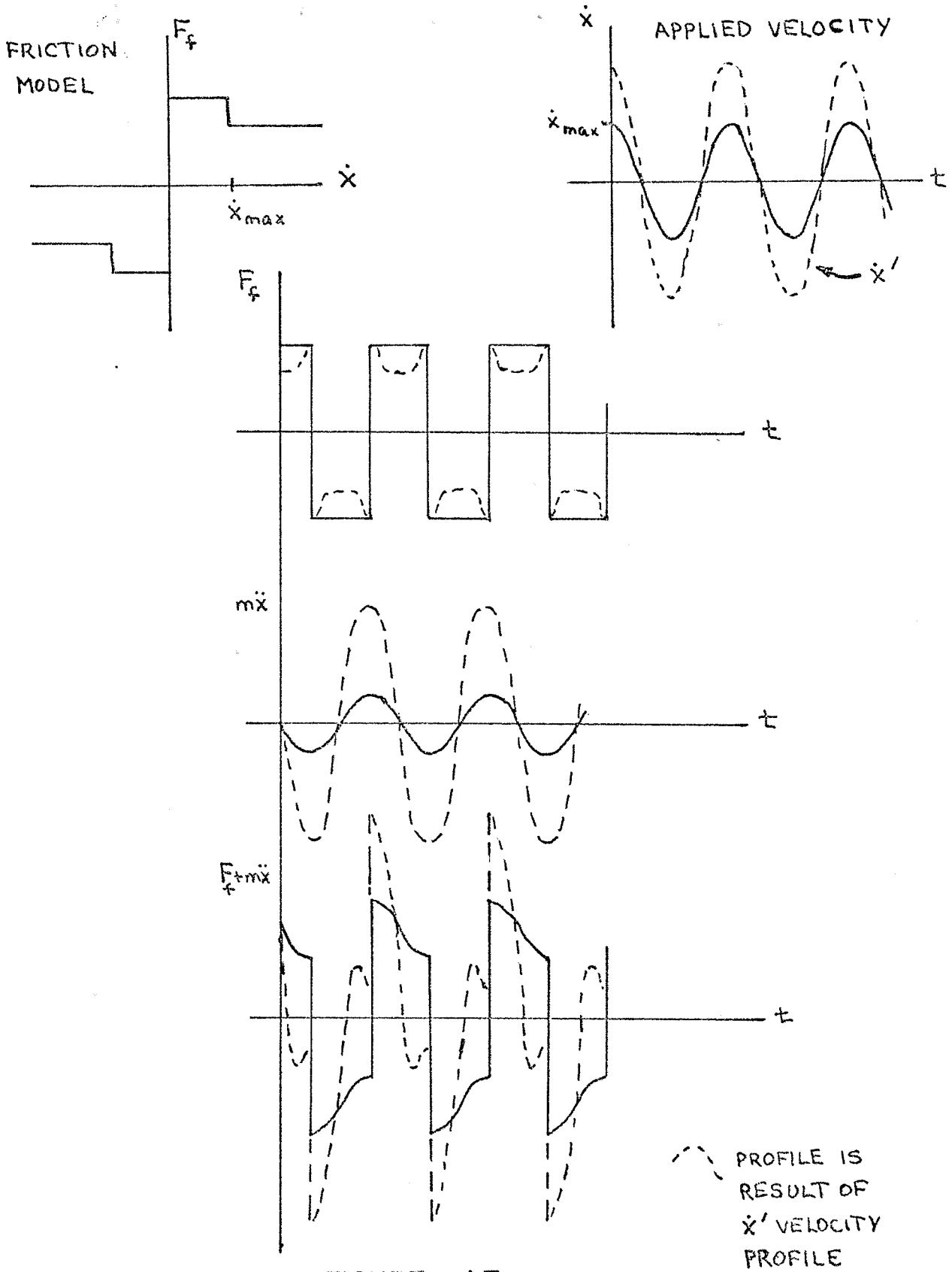
FRICTION MODEL
F_f
$\dot{x}$
$\dot{x}_{max}$
$\dot{x}$
APPLIED VELOCITY
$\dot{x}_{max}$
t
$\dot{x}'$
F_f
t
$m\ddot{x}$
t
$F_f + m\ddot{x}$
t
PROFILE IS RESULT OF $\dot{x}'$ VELOCITY PROFILE

FIGURE 17

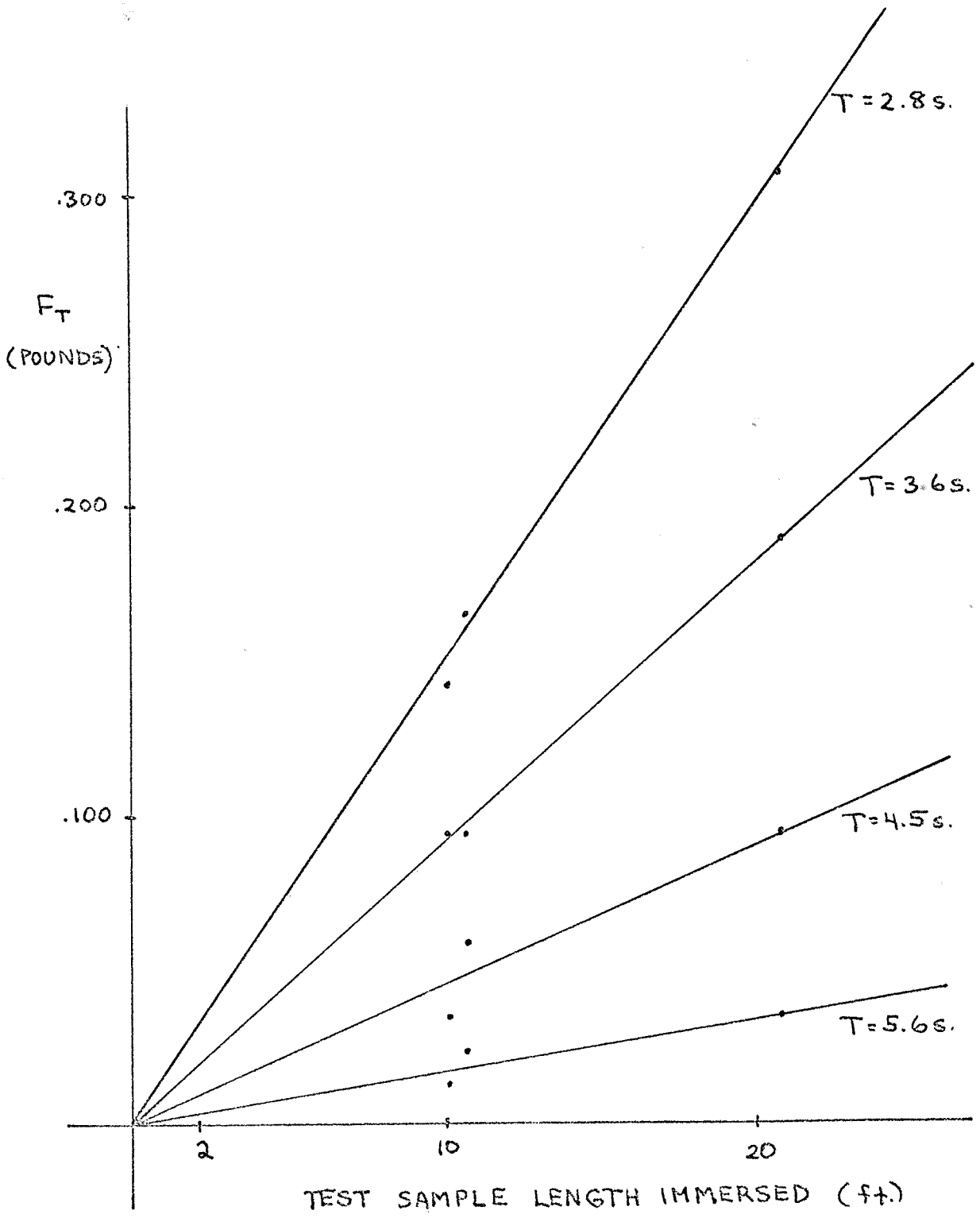
T = 2.8 s.
T = 3.6 s.
T = 4.5 s.
T = 5.6 s.
.300
.200
.100
F_T
(POUNDS)
2
10
20
TEST SAMPLE LENGTH IMMERSED (ft.)

FIGURE 18

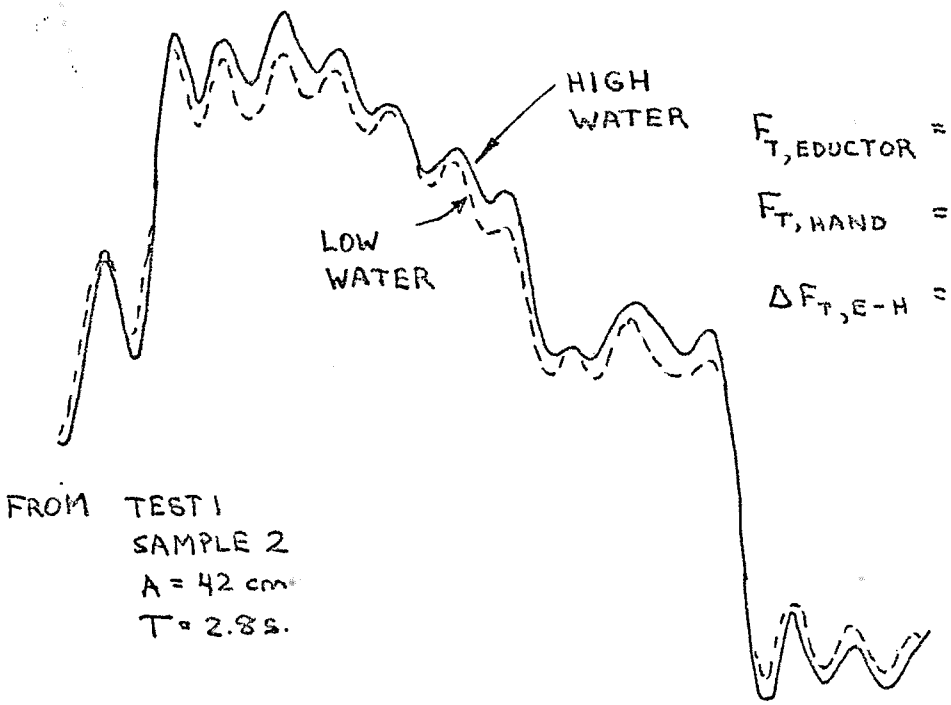
HIGH WATER
LOW WATER
$F_{T,EDUCTOR}$ = .372 lbs.
$F_{T,HAND}$ = .413 lbs.
$\Delta F_{T,E-H}$ = -.041 lbs.
FROM TEST 1
SAMPLE 2
A = 42 cm
T = 2.8 s.

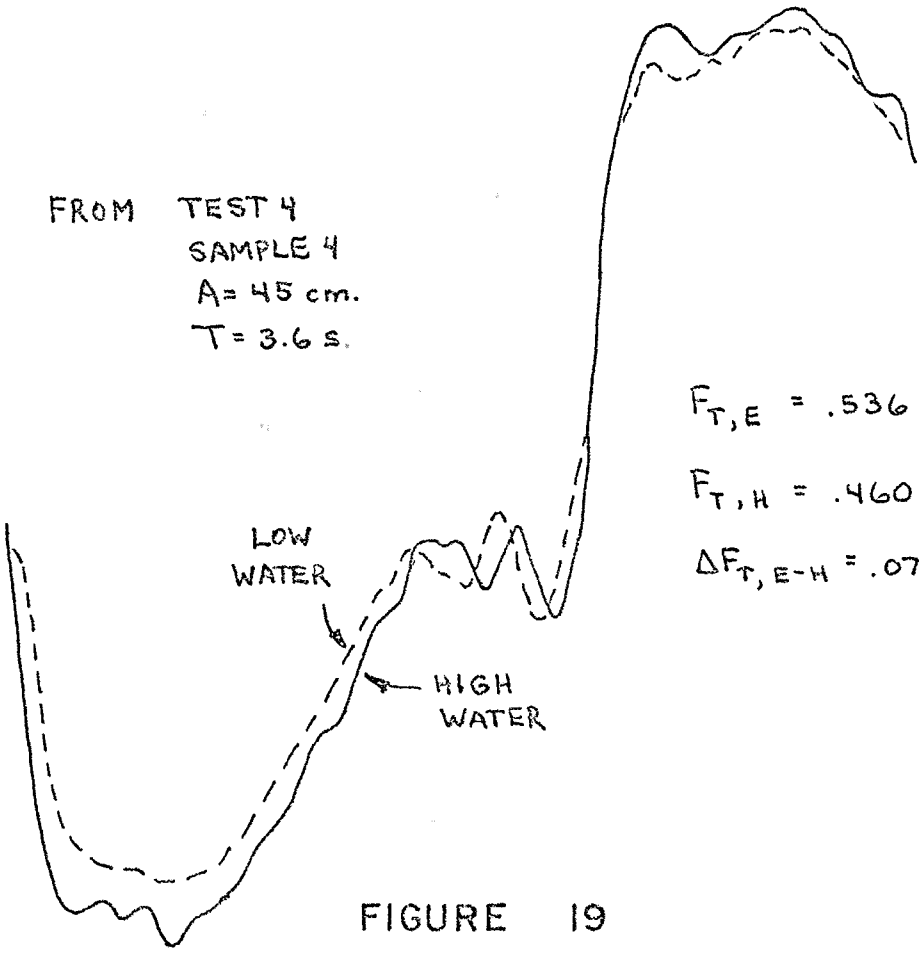
FROM TEST 4
SAMPLE 4
A = 45 cm.
T = 3.6 s.
$F_{T,E}$ = .536 lbs.
$F_{T,H}$ = .460 lbs.
$\Delta F_{T,E-H}$ = .076 lbs.
LOW WATER
HIGH WATER

FIGURE 19

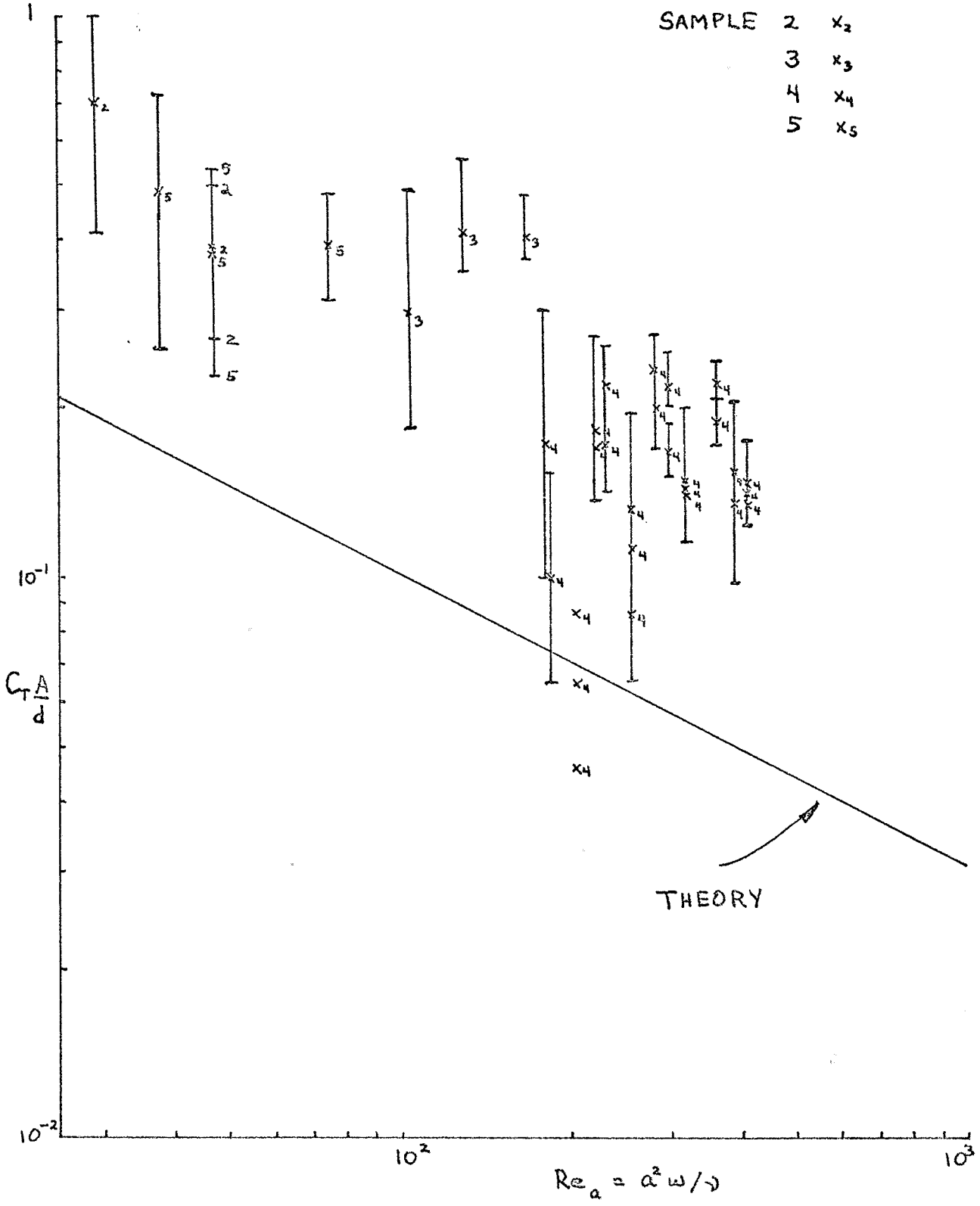

FIGURE 20

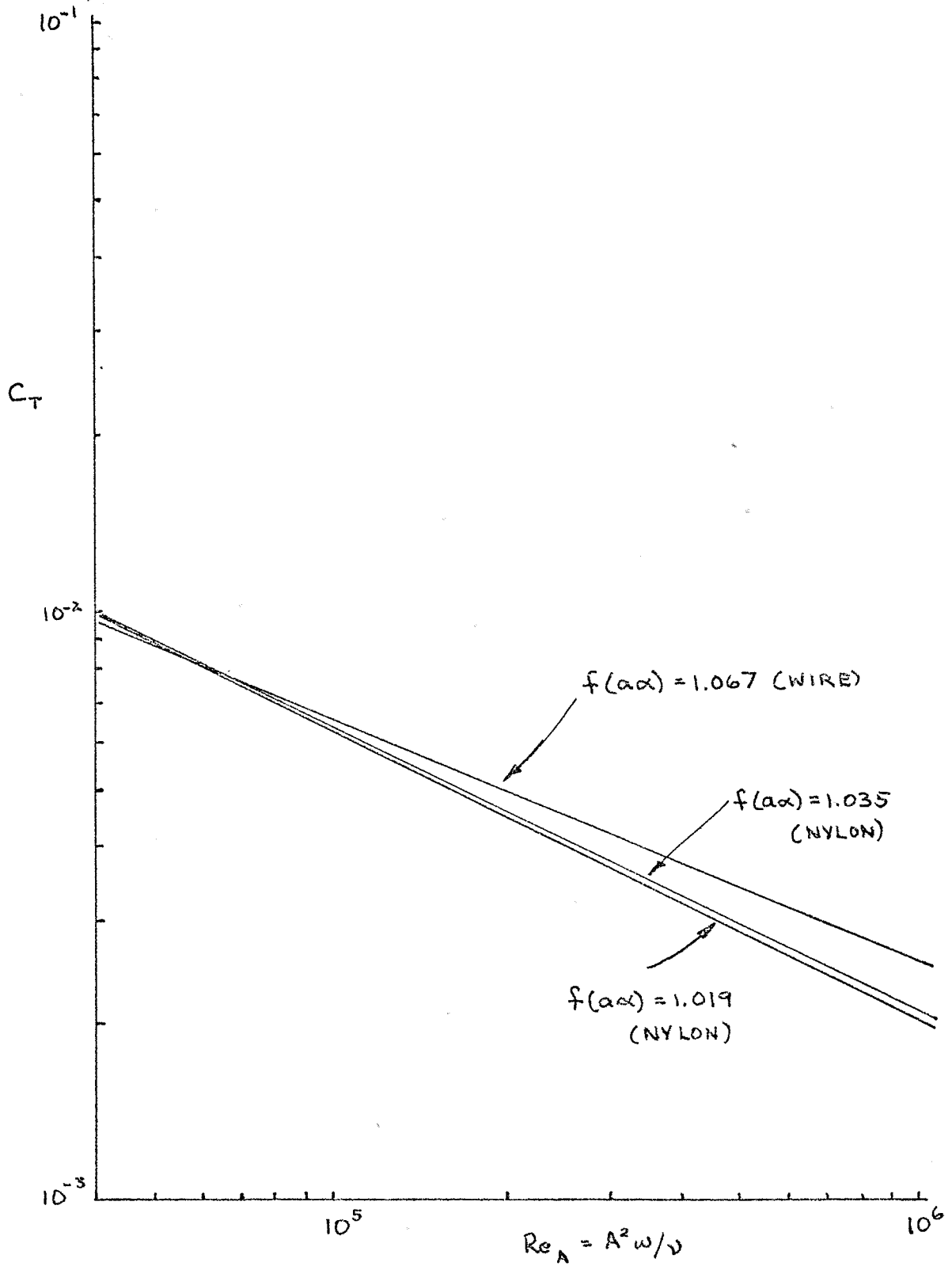
10^{-1}
C_T
10^{-2}
10^{-3}
$f(a\alpha) = 1.067$ (WIRE)
$f(a\alpha) = 1.035$
(NYLON)
$f(a\alpha) = 1.019$
(NYLON)
10^5
10^6
$Re_A = A^2\omega/\nu$

FIGURE 21

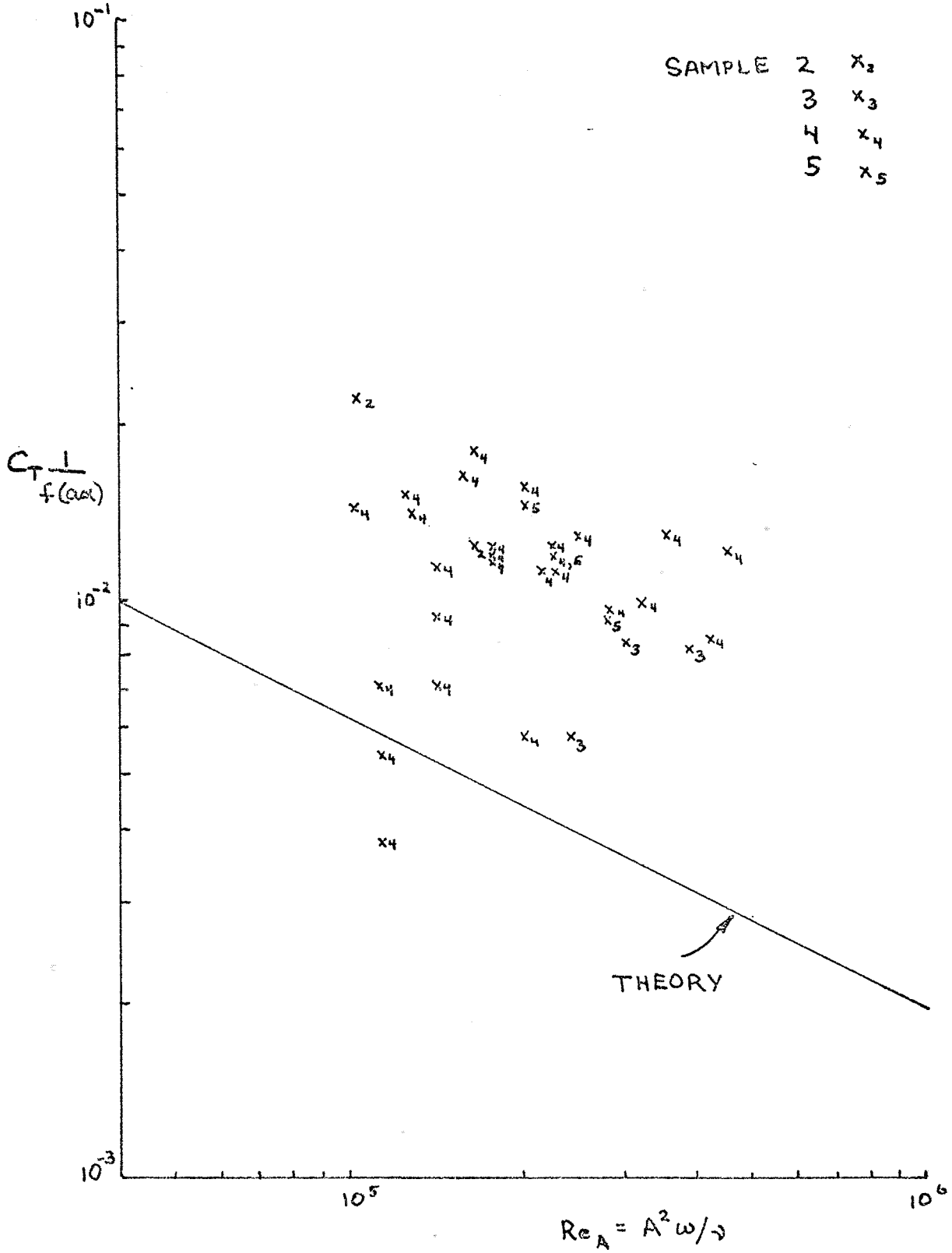
SAMPLE 2 x2
3 x3
4 x4
5 x5
$C_T \frac{1}{f(\alpha\omega)}$
10^{-1}
10^{-2}
10^{-3}
10^5
10^6
$Re_A = A^2\omega/\nu$
THEORY

FIGURE 22

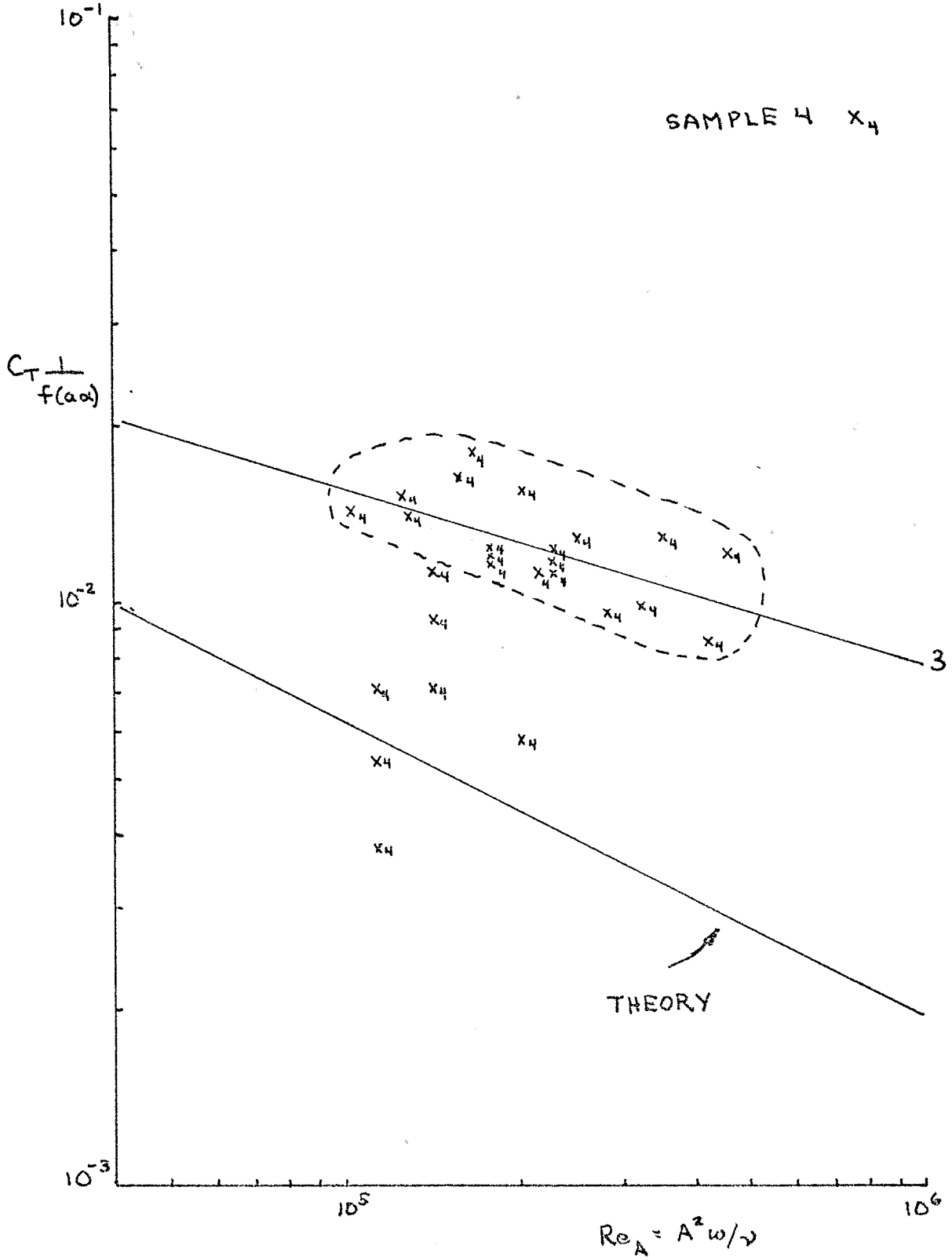
SAMPLE 4 X_4
10^{-1}
10^{-2}
10^{-3}
$C_T \frac{1}{f(a\alpha)}$
3
THEORY
10^5
10^6
$Re_A = A^2\omega/\nu$

FIGURE 23

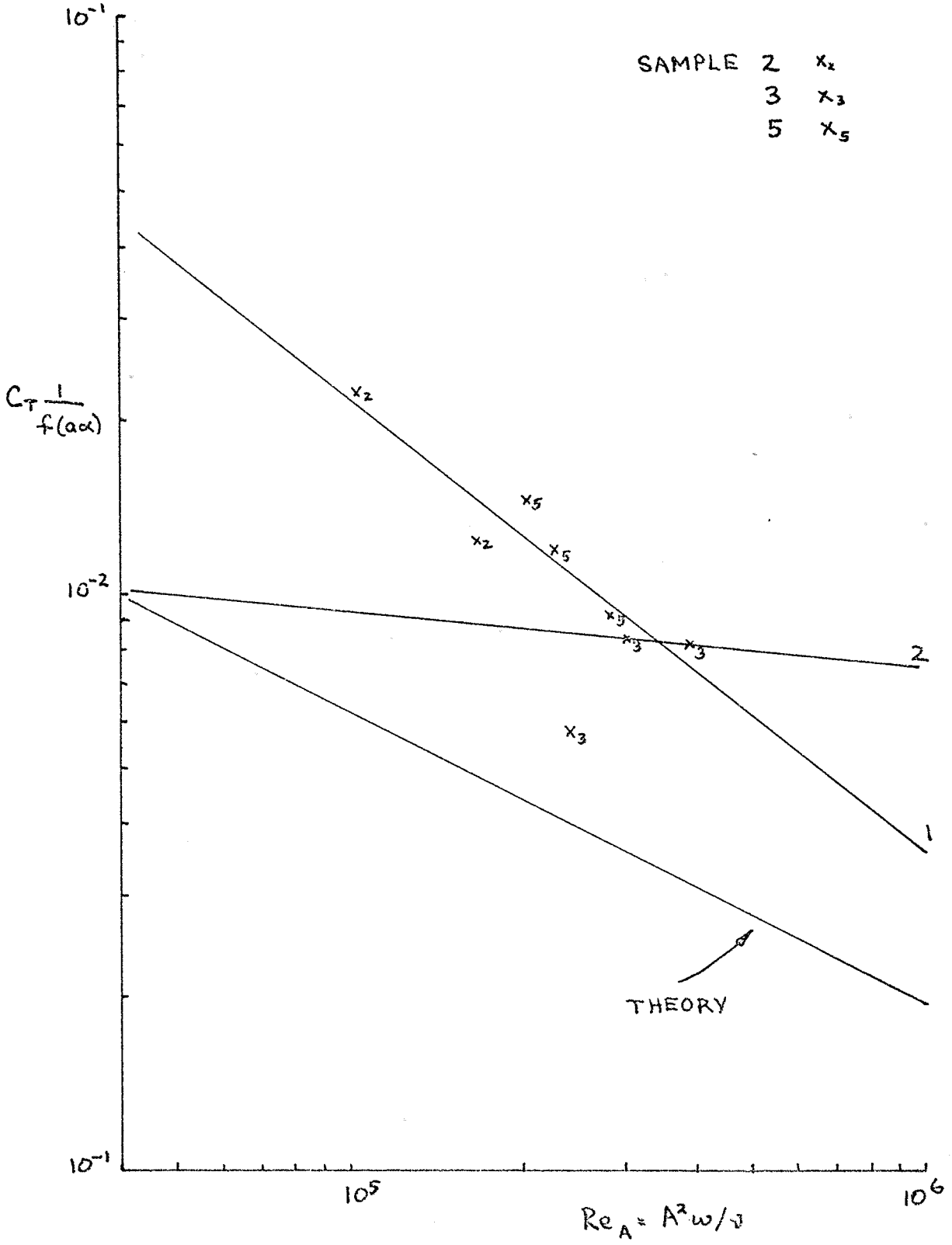
SAMPLE 2 x_2
3 x_3
5 x_5
10^{-1}
$C_T \frac{1}{f(a\alpha)}$
10^{-2}
10^{-1}
10^5
10^6
$Re_A = A^2\omega/\nu$
THEORY
1
2

FIGURE 24

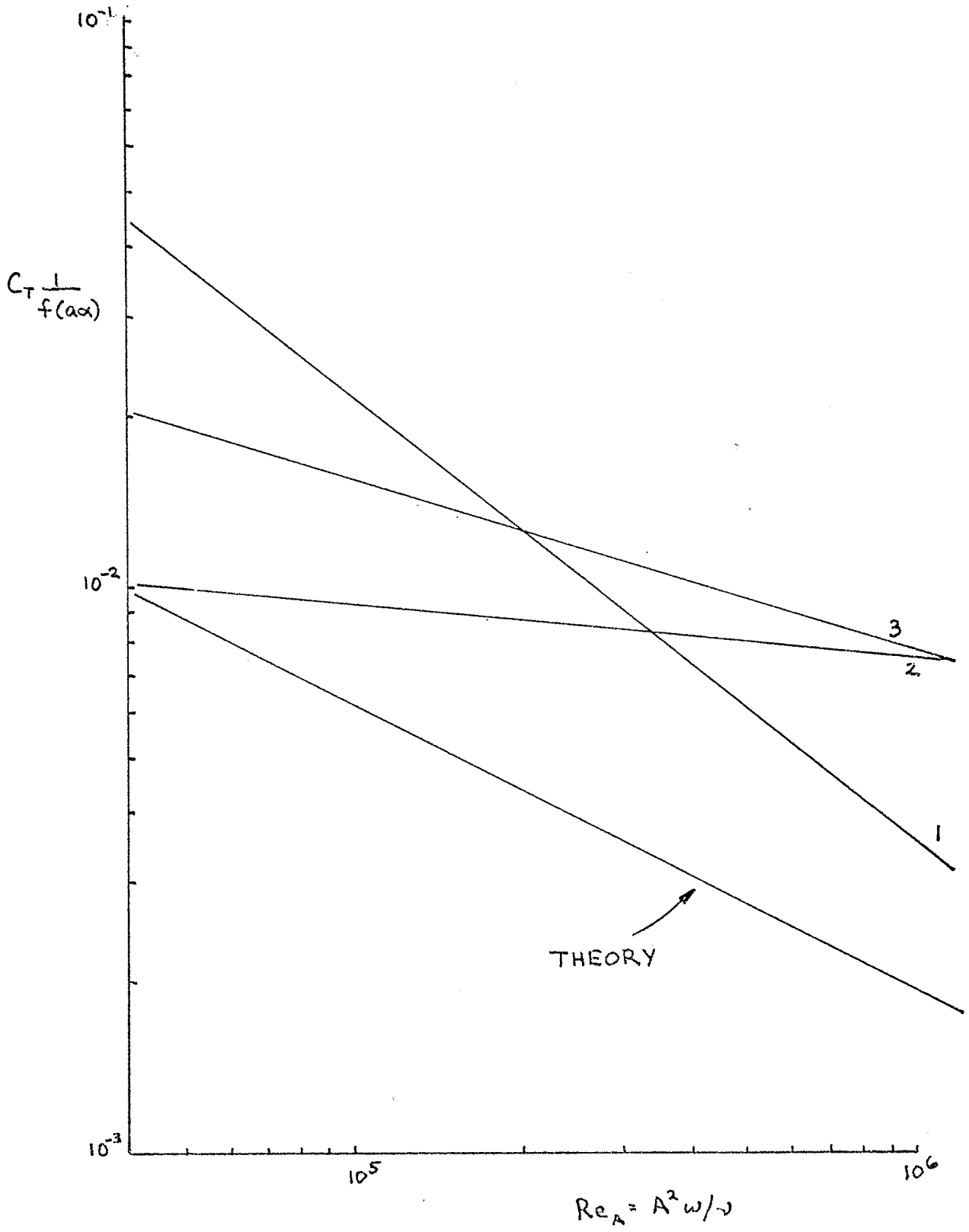
10^{-1}
$C_T \frac{1}{f(a\alpha)}$
10^{-2}
10^{-3}
3
2
1
THEORY
10^5
10^6
$Re_A = A^2\omega/\nu$

FIGURE 25

APPENDIX I

The following four equations are the Navier-Stokes and continuity equations expressed in circular cylindrical coordinates (r, θ, z) with velocities (V_r, V_θ, V_z), (Schlichting, 1968):

(A1)
$$\rho \left(\frac{\partial V_r}{\partial t} + V_r \frac{\partial V_r}{\partial r} + \frac{V_\theta}{r} \frac{\partial V_r}{\partial \theta} - \frac{V_\theta^2}{r} + V_z \frac{\partial V_r}{\partial z}\right)$$
$$= F_r - \frac{\partial p}{\partial r} + \mu \left(\frac{\partial^2 V_r}{\partial r^2} + \frac{1}{r} \frac{\partial V_r}{\partial r} - \frac{V_r}{r^2} + \frac{1}{r^2} \frac{\partial^2 V_r}{\partial \theta^2} - \frac{2}{r^2} \frac{\partial V_\theta}{\partial \theta} + \frac{\partial^2 V_r}{\partial z^2}\right)$$

(A2)
$$\rho \left(\frac{\partial V_\theta}{\partial t} + V_r \frac{\partial V_\theta}{\partial r} + \frac{V_\theta}{r} \frac{\partial V_\theta}{\partial \theta} + \frac{V_r V_\theta}{r} + V_z \frac{\partial V_\theta}{\partial z}\right)$$
$$= F_\theta - \frac{1}{r} \frac{\partial p}{\partial \theta} + \mu \left(\frac{\partial^2 V_\theta}{\partial r^2} + \frac{1}{r} \frac{\partial V_\theta}{\partial r} - \frac{V_\theta}{r^2} + \frac{1}{r^2} \frac{\partial^2 V_\theta}{\partial \theta^2} + \frac{2}{r^2} \frac{\partial V_r}{\partial \theta} + \frac{\partial^2 V_\theta}{\partial z^2}\right)$$

(A3)
$$\rho \left(\frac{\partial V_z}{\partial t} + V_r \frac{\partial V_z}{\partial r} + \frac{V_\theta}{r} \frac{\partial V_z}{\partial \theta} + V_z \frac{\partial V_z}{\partial z}\right)$$
$$= F_z - \frac{\partial p}{\partial z} + \mu \left(\frac{\partial^2 V_z}{\partial r^2} + \frac{1}{r} \frac{\partial V_z}{\partial r} + \frac{1}{r^2} \frac{\partial^2 V_z}{\partial \theta^2} + \frac{\partial^2 V_z}{\partial z^2}\right)$$

(A4)
$$\frac{\partial V_r}{\partial r} + \frac{V_r}{r} + \frac{1}{r} \frac{\partial V_\theta}{\partial \theta} + \frac{\partial V_z}{\partial z} = 0$$

APPENDIX 2

In order to design the ring dynamometer, it is necessary to predict the maximum force that might be felt in the ring. The force that contributes most to the total force felt in the ring is the inertia force, with the friction force and the (hydrodynamic) tangential drag force and surface piercing force being almost negligible by comparison. Presumably the friction force is small, but out of curiosity it will be calculated here. First the inertia forces will be evaluated, followed by the friction forces.

A. Inertia forces

The total inertia force of the system is due to two main components of the system; the four PVC pulleys and the test sample of line. The mass of the forcing rod itself is insignificant or the forcing rod would also have to be included as contributing to the system inertia.

1. Pulleys

$\rho_{PVC} = 2.7$ slugs/ft.^{3}

volume/pulley $\simeq \frac{\pi D^2}{4} t_p = .0654$ ft.^{3}

where $t_p = 1$ inch, the thickness of the pulley

$D = 12$ inches, the pulley diameter .

So for four pulleys, total mass m_p becomes

$m_p = .706$ slugs .

The pulleys are being rotated, not translated, so the maximum inertia force F_p becomes

$$F_p = \frac{I\ddot{\theta}}{D/2}$$

where $I = \frac{m_p(D/2)^2}{2}$, the polar moment of inertia of the pulleys

$\ddot{\theta} = \frac{A\omega^2}{D/2}$, the angular acceleration of the pulleys.

So,

$$F_p = \frac{m_p A\omega^2}{2}$$

For $A\omega^2_{max} = 7.55$ ft./s^2, F_p becomes

$F_p = 2.66$ pounds .

2. Heaviest test sample - Sample 4

dry weight/ft. = .260 pounds/ft. (Table 1)

sample length = 33.5 ft.

So the mass of the sample m_s becomes

$m_s = .272$ slugs .

The peak translational inertia force F_s for $A\omega^2_{max}$ becomes

$F_s = m_s A\omega^2_{max}$

$F_s = 2.05$ pounds .

So the total maximum inertia force F_i for the system is

$F_i = F_p + F_s = 4.72$ pounds .

B. Friction forces

The friction force in the system is due mainly to the friction in the needle bearings in the pulleys. Assigning a relatively large friction coefficient (for needle bearings) to the bearings (Shigley, 1963), the friction force is calculated below:

The friction torque T_f is defined as (Shigley, 1963)

$$T_f = \frac{c_f R_T B}{2}$$

where c_f = .010, friction coefficient

$R_T = T_0\sqrt{2}$, the radial bearing load

T_0= 50 pounds, the tension in the test sample

B = .5 inches, bearing bore

So,

$$T_f = .177 \text{ inch-pounds} .$$

Four four pulleys, each with a radius $\frac{D}{2}$ = 6 inches, the friction force becomes

$$F_f = \frac{4T_f}{D/2} = .118 \text{ pounds} .$$

Obviously the friction force is small for nearly ideal needle bearings.

The following friction calculations are done with hindsight; after performing the experiments and observing a friction-dominated waveform, it is interesting to backfigure and try to evaluate the real friction coefficient that was encountered. The maximum observed static friction was on the order of four pounds, so

$$F_f = 4 \text{ pounds} = \frac{4T_f}{D/2} = \frac{4c_f RB}{D}$$

Then solving for c_f,

$$c_f = \frac{F_f D}{4RB} = .34 .$$

The observed friction coefficient was more than one order of magnitude larger than the textbook value of the friction coefficient for needle bearings.

APPENDIX 3

The ring dynamometer design was based on three considerations: first, it had to be designed so that the maximum force conditions would not cause failure or inelastic behavior of the ring. To preclude failure or inelastic behavior, aluminum with a very high tensile strength, Al 7075 T6, was used as the ring material, and its yield strength is 70,000 pounds per square inch (psi). Secondly, the ring had to be sensitive enough to resolve the forces caused by the hydrodynamic drag being studied. This design requirement has to do with the strain gages and output device; in conjunction with the SR-4 strain gages on aluminum, the MFE chart recorder with its highest sensitivity setting was capable of producing a 3 mm deflection per 1000 psi of applied stress. The chart paper width was 50 mm and the next highest sensitivity was 1.5 mm/1000 psi. And the third consideration was that the ring not be of dimensions that made it too difficult to fabricate.

After sample calculations were performed to have a better understanding of the stress-strain equations for the ring geometry, a ring radius R = 2.25 inches, width w = .5 inches, and thickness t = .0625 inches were chosen after some juggling of parameters to meet all three design requirements. The following calculations apply to a ring with strain gages placed 90 degrees from the axis of the force F (see Figure 6); the moment M in the ring at the 90 degree point becomes (Roark, 1965),

$$M = .1817\ F\ R$$

$$= .4088\ F, \quad \text{for } R = 2.25 \text{ inches} .$$

The stress σ is

$$\sigma = \frac{Mc}{I}$$

where $$c = \frac{t}{2}$$

$$I = \frac{w\, t_3}{12}$$

so that

$$\sigma = \frac{12M}{t^2}$$

$$= 4.9056\, \frac{F}{t^2}$$

$$= 1255.8\, F$$

The resulting MFE chart recorder deflections are listed for several load forces F, as follows:

F (lbs.)	(psi)	deflection (mm)
15	18,837	56.51
10	12,558	37.67
5	6,279	18.84
1.5	1,884	5.65
.15	188	.56

Based on the three design criteria, the dimensions given above were chosen as being satisfactory. If high forces; i.e., forces greater than about 6.5 pounds, were encountered, the chart recorder sensitivity could be lowered. But if the forces were less than 6.5 pounds, the highest

sensitivity setting could be used with single amplitude forces causing chart recorder deflections that would not exceed 25 mm. Even a force as large as 15 pounds would not cause the ring to be near failure or near a region of inelastic behavior. And a 1/16th (.0625) inch wall thickness, although somewhat difficult to machine, would not be impossible to work with.

The actual ring dimensions after machining were

$R = 2.266$ inches

$w = .531$ inches

$t = .0618$ inches .

APPENDIX 4

The following calculations predict the tension needed in the test samples in order to prevent transverse vibrations in the 12-foot vertical test sample sections for the experimental oscillation frequencies:

Using the wave equation we find that

$$\frac{\partial^2 y}{\partial t^2} = \frac{T_o}{\rho S} \frac{\partial^2 y}{\partial x^2}$$

where y is the line deflection

x is the distance along the line

ρ is the line density

S is the line cross sectional area

T_o is the tension in the line

or

$$\frac{\partial^2 y}{\partial t^2} = c^2 \frac{\partial^2 y}{\partial x^2}$$

where $c = \sqrt{\frac{T_o}{\rho S}}$ is the wavespeed,

The natural frequency of vibration ω_n is given by

$$\omega_n = \frac{n\pi}{l}\sqrt{\frac{T_o}{\rho S}} = \frac{n\pi}{l} c$$

where $n = 1, 2, 3, ...$

l = line length = 12 feet .

We would like to determine the minimum tension T_o so that $\omega_n >> 2.244$ rad./s, the highest oscillation frequency, for all test samples. So

$$T = \left(\frac{\omega_n l}{n\pi}\right)^2 \rho S$$

$$T_{min} = \left(\frac{\omega l}{\pi}\right)^2 (\rho S)_{max}$$

For $(\rho S)_{max}$ = .0081 slugs/ft. for Sample 4 (see Table 1), if ω = 10 rad./s, then T_{min} = 12 pounds, and if ω = 22 rad./s, then T_{min} = 57 pounds. So depending on the definition of "much greater than", the choice of tension can vary considerably. Fifty pounds was felt to be a good choice.